

Multi-kinks and composite oscillons in a commensurable and non degenerate double sine-Gordon model

Jonathan Lozano-Mayo,^a Manuel Torres-Labansat,^{b,1}

^a Weinberg Institute for Theoretical Physics, Department of Physics, The University of Texas at Austin, Austin, TX 78712, USA

^b Instituto de Física, Universidad Nacional Autónoma de México, Apartado Postal 20-364, Ciudad de México 01000, México

E-mail: Jonathanloz@utexas.edu, torres@fisica.unam.mx

ABSTRACT: In this paper, we introduce a commensurable and non-degenerate double sine-Gordon model, in which a partial breaking of vacuum degeneracy provides a mechanism for the emergence of static multi-kinks. These multi-kinks K_n are stable field configurations with internal structure, consisting of n localized energy packets with well-defined separations. The properties of the multi-kinks are thoroughly analyzed, including the novel phenomenology that arises during their collisions. In particular, we observe the emergence of long-lived composite oscillons that reflect the original structure of the multi-kinks. The sub-kink's positions and their vibration modes provide collective coordinates that are used to construct a phenomenological model, which offers a good qualitative explanation of the observed oscillon properties. Radiation effects are consistently incorporated, revealing that they play an important role in the observed synchronization of the oscillon's vibrational components.

KEYWORDS: Generalized sine-Gordon models, multi-kinks, composite oscillons, collective coordinate model

¹Corresponding author.

Contents

1	Introduction	1
2	The commensurable and non degenerate double sine-Gordon model	3
2.1	General considerations	3
2.2	The potential	3
2.3	n kinks k_i in the $\alpha = 0$ degenerate regime	5
2.4	Multi-kink K_n in the $\alpha > 0$ non-degenerate regime	6
2.4.1	Multi-kink mass $M_{K_{(n,\alpha)}}$	7
2.4.2	Multi-kink profile $\Phi_n(z)$ and size $\sigma_{K_{(n,\alpha)}}$	8
2.5	Sub-kinks and multi-kink spectra	11
3	Collective coordinate model	13
3.1	Forces between $k_i - k_{i+1}$ sub-kinks	13
3.2	Force between K_n and \bar{K}_n multi-kinks	15
3.3	Radiation energy losses	16
3.4	Equations of motion	18
4	Multi-kink collisions	21
4.1	$K_n - K_n$ collisions	22
4.2	$K_n - \bar{K}_n$ collisions	22
5	Conclusions	29

1 Introduction

Scalar field theories provide a versatile framework for modeling a wide variety of physical phenomena. In particular, they offer a natural setting for spontaneous symmetry breaking, a mechanism that underlies both phase transitions and the generation of particle masses through the Higgs mechanism. In the standard picture, spontaneous symmetry breaking arises as a control parameter of the potential is varied, producing multiple degenerate vacua. In some models, tuning an additional parameter can partially lift this degeneracy. The present work is devoted to exploring the dynamical consequences of such situations.

A distinctive feature of nonlinear scalar field theories is their ability to support solitons: spatially localized, stable, finite-energy configurations having a conserved topological charge [1–3]. Even the simplest one-dimensional example, the ϕ^4 model with two degenerate minima, exhibits kink solutions whose dynamics remain an active subject of study [4–6]. Of particular interest are kink-antikink collisions. At low impact velocities these typically produce long-lived bound states, or bions [7]. At higher velocities, collisions may lead to

inelastic reflections in which the solitons escape to infinity after undergoing several bounces. The resulting outgoing-incoming velocity diagrams display resonance windows characteristic of chaotic scattering [5, 8–10]. Much of this phenomenology can be qualitatively captured by reducing the full field theory to a small number of collective coordinates, most commonly the kink position and its internal (shape) mode. In this description, multi-bounce events arise from reversible energy exchange between translational and vibrational modes [11–14].

Another paradigmatic example is the sine-Gordon (SG) model [15, 16], an exactly integrable system whose analytical solutions can be constructed using the inverse scattering method [17, 18]. Besides static kinks, the SG model admits breathers and multi-soliton solutions, in which scattering occurs without radiation and solitons emerge unchanged apart from a phase shift. Many generalizations of sine-Gordon theory have been explored extensions that break exact integrability but retain some SG-like characteristics [19].

Models featuring multiple degenerate vacua have also attracted significant attention. The ϕ^6 model is one of the most studied examples, with extensive analyses of its kink-antikink dynamics and resonance structure [20–23]. Similar models are relevant for describing both first- and second-order phase transitions [24, 25], as well as long-range and non-exponential inter-kink forces [26–29]. Some of the aforementioned models support multi-kink solutions with internal structure [21, 30–34].

Nonlinear scalar theories also host oscillons: spatially localized, quasi-periodic, exceptionally long-lived configurations despite having no conserved topological charge. Beyond their intrinsic mathematical interest, oscillons appear in diverse high energy physics and cosmological scenarios, including post-inflationary reheating and phase-transition dynamics (see, e.g., [35–39]).

In this work we introduce a commensurable and non-degenerate double K_n sine-Gordon model, which naturally brings together many of the themes mentioned above. In this model, the usual sine-Gordon potential is modulated by a second periodic term, effectively extending the periodicity from $\phi \rightarrow \phi + 2\pi$ to $\phi \rightarrow \phi + 2\pi n$. This structure produces n inequivalent kink solutions k_i , $i = 1, \dots, n$. Introducing a degeneracy-breaking parameter α lifts the degeneracy between internal vacua while preserving the external ones, causing the individual kinks to merge into a single composite multi-kink configuration denoted as K_n .

Exact analytic expressions for K_n are not available, but we derive accurate approximate profiles that closely match the numerical solutions. These enable a detailed study of the multi-kink's structure, including inter-kink forces, equilibrium separations, topological charge, size, and mass.

We also investigate multi-kink collisions. By varying the degeneracy-breaking parameter α and the initial impact velocity, we uncover a diverse range of outcomes: inelastic reflections, annihilation processes, and the formation of long-lived composite oscillons.

To interpret these results, we develop an effective collective coordinate model based on the positions $x_i(t)$ of the internal kinks and their vibrational modes. Crucially, we show that including radiation effects in the effective theory is essential to reproduce the synchronization phenomena observed in the oscillon dynamics of the full field theory.

The paper is organised as follows. Section 2 introduces the commensurable and non-degenerate double sine-Gordon model. Section 3 presents the derivation of the collective coordinate model. Section 4 analyzes collisions of the K_4 multi-kink with its corresponding \bar{K}_4 anti-multi-kink. Final remarks are given in Section 5.

2 The commensurable and non degenerate double sine-Gordon model

2.1 General considerations

The Lagrangian density for the scalar field $\phi(t, z)$ is

$$\mathcal{L} = \frac{1}{2} \left(\frac{\partial \phi}{\partial t} \right)^2 - \frac{1}{2} \left(\frac{\partial \phi}{\partial z} \right)^2 - V_{n,\alpha}. \quad (2.1)$$

Thus, the energy functional corresponding to this Lagrangian is given by the following expression

$$E[\phi] = \int_{-\infty}^{\infty} \mathcal{E}(t, z) dz = \int_{-\infty}^{\infty} \left(\frac{1}{2} \left(\frac{\partial \phi}{\partial t} \right)^2 + \frac{1}{2} \left(\frac{\partial \phi}{\partial z} \right)^2 + V_{n,\alpha} \right) dz, \quad (2.2)$$

whereas the field equation of motion is given as

$$\frac{\partial^2 \phi}{\partial t^2} - \frac{\partial^2 \phi}{\partial z^2} = -\frac{dV_{n,\alpha}}{d\phi}. \quad (2.3)$$

Focusing on static configurations, the previous equation becomes

$$\frac{d^2 \phi}{dz^2} = \frac{dV_{n,\alpha}}{d\phi}, \quad (2.4)$$

multiplying this equation by $d\phi/dz$ and integrating yields the first order Bogomol'nyi equation [40]

$$\frac{1}{2} \left(\frac{d\phi}{dz} \right)^2 = V_{n,\alpha}(\phi), \quad (2.5)$$

where the integration constant is selected as zero, so the kink energy obtained from Eq.(2.2) is finite. We find convenient to define the superpotential $W_{n,\alpha}(\phi)$ [41, 42] as

$$W_{n,\alpha}(\phi) = \int^{\phi} \sqrt{2V_{n,\alpha}(\phi)} d\phi, \quad (2.6)$$

this expression together with the Bogomol'nyi Eq.(2.5) imply the relation $(d\phi/dz) = (dW_{n,\alpha}/d\phi)$.

2.2 The potential

In the proposed model the usual Sine-Gordon potential $(1 - \cos \phi)$ is modulated by a second Sine-Gordon-like term $\left(1 + \cos \frac{\phi}{n}\right)$ and shifted by the degeneracy-breaking parameter α . As a result, the potential

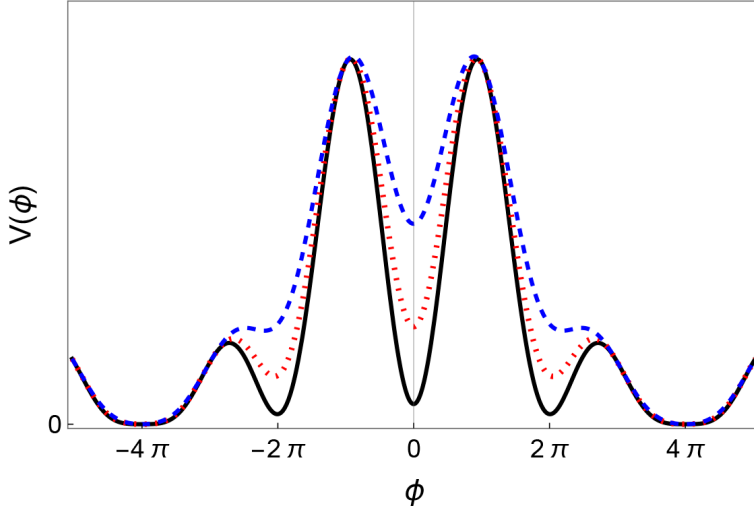


Figure 1. Potential $V_{n,\alpha}(\phi)$, the parameters are selected as: $n = 4$, with: $\alpha = 0.1$ (black-continuous line), $\alpha = 0.6$ (red-dotted line) and $\alpha = 1.5$ (blue-dashed line).

$$V_{n,\alpha}(\phi) = \frac{1}{2(1 + \frac{1}{2}|\alpha|)} (1 - \cos \phi + \alpha) \left(1 + \cos \frac{\phi}{n}\right), \quad (2.7)$$

takes the form shown in Fig. (1). For future reference, it is convenient to split the potential as $V_{n,\alpha}(\phi) = V_{n,0}(\phi) + \alpha \Delta_{n,\alpha}(\phi)$, with

$$\Delta_{n,\alpha}(\phi) = \frac{2}{2 + \alpha} \left(\cos \frac{\phi}{2} \cos \frac{\phi}{2n} \right)^2. \quad (2.8)$$

The potential reduces to the usual Sine-Gordon form when $\alpha = 0$ and $n \rightarrow \infty$. In the opposite limit, as $\alpha \rightarrow \infty$, it also approaches a SG potential under the field redefinition $\phi \rightarrow \frac{\phi}{n} + \pi$. The potential $V_{n,\alpha}$ is invariant under the transformations $\phi \rightarrow -\phi$ and $\phi \rightarrow \phi + 2\pi n$. Unless otherwise specified, we focus on solutions within the sector $\phi \in \{-\pi n, \pi n\}$ sector. For simplicity, we assume that n is an even integer, similar results hold for odd n .

The $n+1$ potential minima can be determined numerically, a useful analytical approximation can be obtained in the small- α regime

$$v_i \approx 2i\pi + \frac{\alpha \sin\left(\frac{2\pi i}{n}\right)}{2n \cos^2\left(\frac{\pi i}{n}\right)}, \quad i = \pm \left(0, 1, 2, \dots, \frac{n}{2} - 1\right), \quad v_{\pm \frac{n}{2}} = \pm n\pi. \quad (2.9)$$

Associated with each potential minimum, there are perturbative scalar excitations whose masses are determined by $m_i = \frac{d^2 V_{n,\alpha}(\phi)}{d^2 \phi} \Big|_{\phi=v_i}$, which, for small α , are approximately given by:

$$m_i \approx \sqrt{\cos^2\left(\frac{i\pi}{n}\right) - \frac{\alpha}{4n^2} \left(6 + n^2 + (n^2 - 4) \cos\left(\frac{2\pi i}{n}\right)\right)}, \quad m_{\pm \frac{n}{2}} = \sqrt{\frac{\alpha}{2n^2}}. \quad (2.10)$$

For $\alpha = 0$, the model admits n kink solutions k_i . As α increases within the $0 < \alpha \leq \alpha_1$ interval, these n kinks merge into a single multi-kink configuration K_n , characterized by

well-defined localized energy lumps. The value α_1 marks the onset of significant overlap among sub-kinks, will be determined later in Eq.(2.26). In the subsequent interval $\alpha_1 < \alpha \leq \alpha_2$, the distinction between individual sub-kinks becomes less pronounced. The α_2 threshold corresponds to the value at which the internal local minima of the potential start disappearing. This critical value can be estimated by requiring that the mass $m_{\frac{n}{2}-1}$ of the internal scalar excitation, given in Eq.(2.10), vanish. This leads to

$$\alpha_2 = \frac{4n^2 \sin^2(\frac{\pi}{n})}{6 + n^2 - (n^2 - 4) \cos(\frac{2\pi}{n})}. \quad (2.11)$$

For $\alpha > \alpha_2$, the field configuration converges to a single soliton, as the internal substructure associated to the multi-kinks is gradually erased. Notice that α_2 has a weak dependence on n , $\alpha_2 \in \{1.6, 1.33\}$ for $n \in \{2, \infty\}$. Although stable soliton solutions are not expected for negative values of α , the model admits the existence of saddle-point solutions that interpolate between false and true vacua. These unstable, energy-maximizing configurations known as sphalerons [42, 43] represent transitions over the potential barrier and will be explored in future work.

2.3 n kinks k_i in the $\alpha = 0$ degenerate regime

For $\alpha = 0$ the potential minima are located at $v_i = 2i\pi$ with $i = \pm(0, 1, 2, \dots, \frac{n}{2})$, so the model admits n kink solutions $\phi_{k_i} \in \{v_i, v_{i+1}\}$, $i = -\frac{n}{2}, \dots, 0, \dots, \frac{n}{2}$, each carrying the same topological charge $q_{k_i} = \frac{1}{2\pi}(v_{i+1} - v_i) = 1$, along with their corresponding antikinks \bar{k}_i , with charge $q_{\bar{k}_i} = -1$. The location of the potential maxima Ω_i deviate from those of the standard sine-Gordon model, where $\Omega_i = \pm(2i - 1)\pi$. In this case, their positions are determined by the solutions to the transcendental equation $n \cot(\frac{\phi}{2}) - \tan(\frac{\phi}{2n}) = 0$. Notice that for $\alpha = 0$, the masses $m_{\pm\frac{n}{2}}$ vanishes.

The superpotential, given in Eq.(2.6) takes the form,

$$W[\phi] = -\frac{4n}{n^2 - 1} \left(n \cos \frac{\phi}{2} \cos \frac{\phi}{2n} + \sin \frac{\phi}{2} \sin \frac{\phi}{2n} \right), \quad (2.12)$$

from which the kink masses are computed as:

$$M_{k_i} = W[v_i] - W[v_{i-1}] = \frac{4n^2}{n^2 - 1} \left(\cos \frac{v_i}{2n} + \cos \frac{v_{i-1}}{2n} \right), \quad i = \pm \left(1, 2, \dots, \frac{n}{2} \right). \quad (2.13)$$

It is interesting to observe that, using Eqs.(2.10,2.13), the masses M_{k_i} are related to the scalar field masses evaluated at the neighboring minima v_i and v_{i-1} through the following expression: $M_{k_i} = \frac{4n^2}{n^2 - 1} (m_i + m_{i-1})$.

The soliton $\phi_{k_i}(z)$ configurations correspond to the solutions of the equation

$$\frac{d\phi}{dz} = 2 \sin \frac{\phi}{2} \cos \frac{\phi}{2n}. \quad (2.14)$$

For $n = 2$, Eq.(2.14) admits the implicit analytical solution $\ln \left[\tan \left(\frac{\phi}{8} \right) \right] + \sec \left(\frac{\phi}{4} \right) = z$. For any other value of n , the equation must be solved numerically. However, a very good analytical approximation can be derived by noting that, within each kink $\phi_{k_i} \in \{v_{i-1}, v_i\}$

sector, the function $\cos \frac{\phi}{2n}$ varies slowly compared to $\sin \frac{\phi}{2}$. This motivates an approach we refer to as the smooth-modulation approximation, which becomes increasingly accurate as n , grows. Under this approximation, if the $\cos \frac{\phi}{2n}$ term is evaluated at the boundary points $\phi \sim v_{i-1}$ or $\phi \sim v_i$, the solutions of Eq.(2.14) coincide with the well known SG field solution with the asymptotic behavior $\phi(z) \sim v_{i-1} + \text{const} e^{m_{i-1} z}$ or $\phi(z) \sim v_i - \text{const} e^{-m_i z}$ as $z \rightarrow \mp\infty$. These results hold for all kinks except those near the absolute minima, where according to Eq.(2.10) the scalar mass $m_{\pm n/2}$ vanishes. In these special cases, the correct asymptotic behavior becomes $\phi(z) \sim \mp n\pi \pm \frac{4n}{z}$. This analysis suggests an ansatz for the kink solution $\phi_{k_i}(z) \in \{v_{i-1}, v_i\}$, that reproduces the correct asymptotic forms in each sector, and is given by

$$\phi_{k_i}(z) = v_{i-1} + 4 \tan^{-1} G_i[z], \quad i = 1, \dots, \frac{n}{2}, \quad (2.15)$$

$$G_i[z] = \frac{1}{a_i e^{-m_{i-1} z} + b_i e^{-m_i z}}, \quad i < \frac{n}{2}, \quad G_{\frac{n}{2}}[z] = \ln \left[1 + \frac{1}{c_n e^{-m_{\frac{n}{2}-1} z} + d_n e^{-z/n}} \right].$$

The solutions for negative values of i are obtained via spatial and field reflection symmetry, using the relation $\phi_{k_{(-i)}}(z) = -\phi_{k_i}(-z)$, $i = 1, \dots, \frac{n}{2}$. Given that $m_{i-1} > m_i$, the $\phi_{k_i}(z)$ ansatz correctly reproduces the asymptotic exponential tails determined by the scalar masses m_{i-1} (for $z \rightarrow -\infty$) and m_i (for $z \rightarrow +\infty$). In the $i = \frac{n}{2}$ case, the function $G_{\frac{n}{2}}[z]$ captures both the exponential $\phi(z) \sim (n-2)\pi + \frac{4}{c_n} e^{-m_{\frac{n}{2}-1} z}$ and long range $\phi(z) \sim n\pi - \frac{4n}{z}$ asymptotic tail behavior. The coefficients a_i , b_i , c_n and d_n are determined by enforcing two conditions: (i) at the kink center the field value matches the location of the potential maxima, *i.e.* $\phi_{k_i}(0) = \Omega_i$, and (ii) the field derivative at this point satisfies Eq.(2.14). Using these conditions, the explicit expressions for the coefficients are derived as

$$a_i = \frac{\gamma_i \mu_i - m_i}{\gamma_i (m_{i-1} - m_i)} \quad b_i = \frac{m_{i-1} - \gamma_i \mu_i}{\gamma_i (m_{i-1} - m_i)}, \quad i = 1, \dots, \frac{n}{2} - 1, \quad (2.16)$$

where $\gamma_i = \tan \frac{\Omega_i - v_{i-1}}{4}$ and $\mu_i = \sin \frac{\Omega_i}{2} \cos \frac{\Omega_i}{2n} / \left(2 \sin^2 \frac{(\Omega_i - v_{i-1})}{4} \right)$, whereas

$$c_n = \frac{n \nu_n - \kappa_n}{n \sin \frac{\pi}{n} - 1} \quad d_n = \frac{n(\kappa_n \sin \frac{\pi}{n} - \nu_n)}{n \sin \frac{\pi}{n} - 1}, \quad (2.17)$$

with $\nu_n = \frac{\kappa_n}{4} (\kappa_n + 1) (1 + \gamma_n^2) \sin \left(\frac{\Omega_{n/2}}{2} \right) \cos \left(\frac{\Omega_{n/2}}{2n} \right)$, $\kappa_n = (e^{\gamma_n} - 1)^{-1}$, and $\gamma_n = \tan \frac{\Omega_{n/2} - (n-2)\pi}{4}$.

Figure (2) presents the $\phi_{k_i}(z)$ kinks profiles obtained from the numerical solutions of Eq.(2.14) as compared with the approximated ansatz Eq.(2.15). The results clearly show that the smooth-modulation approximation performs remarkably well, particularly for $n > 2$.

2.4 Multi-kink K_n in the $\alpha > 0$ non-degenerate regime

In this section, we analyze the properties of the K_n multi-kink that emerges in the $\alpha > 0$ phase. Although the minima v_i are no longer located at integer multiples of 2π , the topological charge Q_n remains straightforward to compute. This is because the values at the absolute minima, $v_{\pm n/2} = \pm n\pi$, are not affected. Consequently, the multi-kink interpolates between $\phi_{z \rightarrow -\infty} = v_{-n/2}$ and $\phi_{z \rightarrow \infty} = v_{n/2}$, yielding a total topological charge

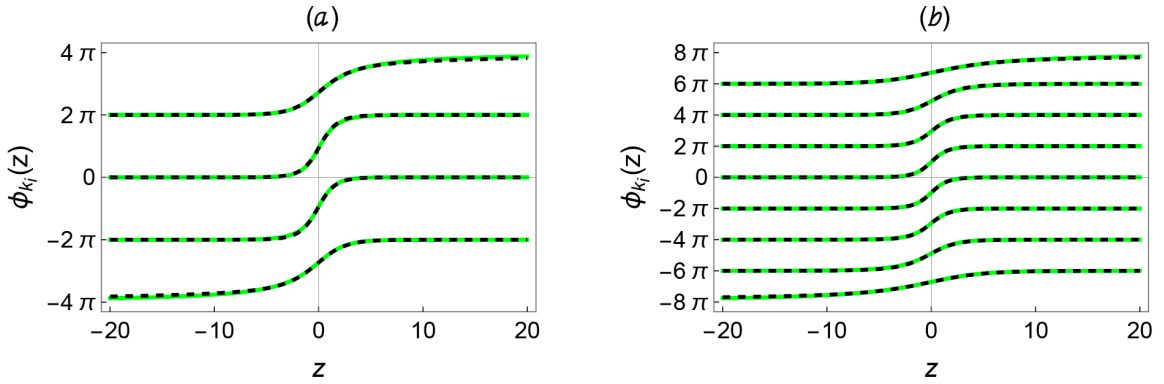


Figure 2. Kink field configurations $\phi_{k_i}(z)$ obtained from the numerical solution of Eq.(2.14) (continuous-green lines) and the approximated ansatz Eq.(2.15) (dashed-black lines); for the (a) $n = 4$ and (b) $n = 8$ cases.

$Q_n = \frac{1}{2\pi}(v_{n/2} - v_{-n/2}) = n$, which corresponds to the sum of the topological charges of the n constituent sub-kinks $Q_n = \sum_i q_{k_i} = n$.

2.4.1 Multi-kink mass $M_{K_{(n,\alpha)}}$

Other multi-kink properties can be analyzed using the smooth-modulation approximation. To compute the total mass $M_{K_{(n,\alpha)}}$, we decompose it into two contributions: the sum of the internal kink masses, $M_{K(n,0)}$, and the α -dependent binding interaction energy, $\Delta_{K(n,\alpha)}$. These correspond to the first and second terms, respectively, in the following expression:

$$M_{K(n,\alpha)} = \int_{-n\pi}^{n\pi} \sqrt{2V_{n,0}(\phi)} d\phi + \int_{-n\pi}^{n\pi} \left(\sqrt{2V_{n,\alpha}(\phi)} - \sqrt{2V_{n,0}(\phi)} \right) d\phi. \quad (2.18)$$

The first term is the sum of the internal kink masses M_{k_i} . Using the results in Eq.(2.13), it follows that

$$M_{K(n,0)} = \sum_{i=-\frac{n}{2}}^{\frac{n}{2}} M_{k_i} = \frac{8n^2}{n^2 - 1} \cot \frac{\pi}{2n}. \quad (2.19)$$

To estimate $\Delta_{K(n,\alpha)}$, the integration domain $\phi \in \{-n\pi, n\pi\}$ is partitioned into n subintervals of the form $\phi \in \{v_i, v_{i+1}\}$. Within each subinterval, the smooth-modulation approximation is applied by taking $1 + \cos(\frac{\phi}{n}) \approx 1 + \cos(\frac{v_i + v_{i+1}}{2n})$, hence $\Delta_{K(n,\alpha)}$ is readily computed as follows:

$$\begin{aligned} \Delta_{K(n,\alpha)} &\approx \sqrt{8} \sum_{i=0}^{\frac{n}{2}-1} \cos \left(\frac{(2i+1)\pi}{2n} \right) \int_{2i\pi}^{2(i+1)\pi} \left(\sqrt{\frac{1+\alpha-\cos\phi}{1+\frac{\alpha}{2}}} - \sqrt{1-\cos\phi} \right) d\phi \quad (2.20) \\ &= \sum_{i=0}^{\frac{n}{2}-1} \cos \left(\frac{(2i+1)\pi}{2n} \right) \left(\sqrt{32} \sqrt{\frac{\alpha}{1+\frac{\alpha}{2}}} \left(E \left[(i+1)\pi, -\frac{2}{\alpha} \right] - E \left[i\pi, -\frac{2}{\alpha} \right] \right) - 16 \right) \\ &= \left(\sqrt{\frac{32\alpha}{1+\frac{\alpha}{2}}} E \left[-\frac{2}{\alpha} \right] - 8 \right) \csc \left(\frac{\pi}{2n} \right). \end{aligned}$$

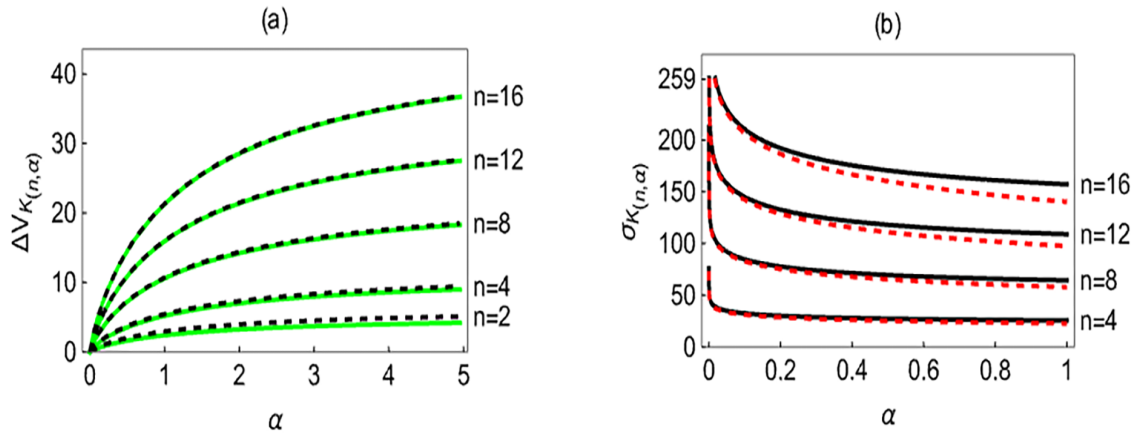


Figure 3. K_n multi-kink: (a) Binding energy $\Delta V_{K(n,\alpha)}$ as a function of α , obtained from the numerical integration of the second term of Eq.(2.18) (continuous-green lines) and the analytical expression in Eq.(2.20) (dashed-black lines). (b) Size $\sigma_{K(n,\alpha)}$ obtained from Eq.(2.29) (continuous-black lines), the dashed lines correspond to the approximated expression in Eq.(2.30).

The integrals involved in the computation are expressed in terms of the incomplete elliptic integral of the second kind, $E[i\pi, -\frac{2}{\alpha}] = 2i E[-\frac{2}{\alpha}]$, evaluated at an argument that simplifies the expression to a complete elliptic integral. This allows us to explicitly evaluate the sum, leading to the final result presented in Eq.(2.20). Figure (3a) compares this analytical approximation with the numerical integration of the second term in Eq.(2.18). The smooth-modulation approximation shows excellent agreement across the entire range of α values.

By adding $M_{K(n,0)}$ and $\Delta_{K(n,\alpha)}$, we obtain the total multi-kink mass:

$$M_{K(n,\alpha)} = \left[\frac{8n^2}{n^2 - 1} \cos\left(\frac{\pi}{2n}\right) + \sqrt{\frac{32\alpha}{1 + \frac{\alpha}{2}}} E\left[-\frac{2}{\alpha}\right] - 8 \right] \csc\left(\frac{\pi}{2n}\right). \quad (2.21)$$

Using the expansion $\sqrt{\frac{32\alpha}{1 + \alpha}} E\left[-\frac{2}{\alpha}\right] - 8 \approx \alpha \left(\ln \frac{32}{\alpha} - 1 \right)$ for $\alpha \ll 1$, the small α limit of Eq.(2.21) yields

$$M_{K(n,\alpha)} \approx \left[\frac{8n^2}{n^2 - 1} \cos\left(\frac{\pi}{2n}\right) + \alpha \ln\left[\frac{12}{\alpha}\right] \right] \csc\left(\frac{\pi}{2n}\right). \quad (2.22)$$

2.4.2 Multi-kink profile $\Phi_n(z)$ and size $\sigma_{K(n,\alpha)}$

Although the mass and charge soliton are well defined for all positive values of α , the emergence of a well-resolved multi-kink structure is restricted to the range $0 < \alpha < \alpha_1$, where α_1 denotes the upper bound beyond which the internal sub-kinks can no longer be clearly distinguished. We now proceed to estimate the value of α_1 .

To begin, note that the separation between adjacent sub-kinks, $\xi_{i+1} - \xi_i$, can be inferred from the Bogomol'nyi equation, Eq. (2.5), under the assumption that each sub-kink is

centered at the point where the field $\phi(z)$ reaches a local maximum of the potential, *i.e.* $\phi(\xi_i) = \Omega_i$. Accordingly [26, 32],

$$\xi_{i+1} - \xi_i = \int_{\Omega_i}^{\Omega_{i+1}} \frac{d\phi}{\sqrt{2[V_{n,\alpha}(\phi)]}}. \quad (2.23)$$

Here $\phi(\xi_i) = \Omega_i$ and $\phi(\xi_{i+1}) = \Omega_{i+1}$ are contiguous maxima of the $V_{n,\alpha}(\phi)$ potential. Recalling that in each region $\phi \in \{\Omega_{i-1}, \Omega_i\}$ the term $1 + \cos\left(\frac{\phi}{n}\right)$ can be approximated as $1 + \cos\left(\frac{\omega_i}{n}\right) = 2m_i^2$, hence a direct integration yields:

$$\xi_{i+1} - \xi_i \approx \frac{1}{2m_i} \int_{\Omega_i}^{\Omega_{i+1}} \sqrt{\frac{1 + \frac{\alpha}{2}}{\frac{\alpha}{2} + \sin^2 \frac{\phi}{2}}} d\phi = \frac{1}{m_i} \sqrt{\frac{2(1 + \frac{\alpha}{2})}{\alpha}} \left(F\left[\frac{\Omega_{i+1}}{2}, -\frac{2}{\alpha}\right] - F\left[\frac{\Omega_i}{2}, -\frac{2}{\alpha}\right] \right), \quad (2.24)$$

where $F[\phi, k]$ is the incomplete elliptic integral function of the first kind. The previous expression can be reduced approximating $\omega_i \approx (2i-1)\pi$, and using the property $F\left[\frac{2i+1}{2}\pi, -\frac{2}{\alpha}\right] = (2i+1)K\left[-\frac{2}{\alpha}\right]$, with $K\left[-\frac{2}{\alpha}\right]$ being the complete elliptic integral function of the first kind, then Eq.(2.24) becomes

$$\xi_{i+1} - \xi_i \approx \frac{2}{m_i} \sqrt{\frac{2(1 + \frac{\alpha}{2})}{\alpha}} K\left[-\frac{2}{\alpha}\right] \approx \frac{1}{m_i} \log\left[\frac{32}{\alpha}\right]. \quad (2.25)$$

Where the last result applies in the $\alpha \ll 1$ limit. We highlight that the $\log\left[\frac{\text{const}}{\alpha}\right]$ dependence for the sub-kinks separation and $\alpha \log\left[\frac{\text{const}}{\alpha}\right]$ for the multi-kink mass are generic results that can be deduced using the thin-wall approximation for scalar field models in which the vacuum degeneracy is partially broken by an small α parameter (see, *e.g.* [21, 30–33]).

The last result in Eq.(2.25) allows us to estimate the condition required for a well-defined multi-kink structure, in which the internal kinks do not significantly overlap. From the analytical expression for $\phi_{k_i}(z)$ in Eq.(2.15), the width σ_{k_i} of the energy density associated with the k_i kink can be estimated as $\sigma_{k_i} = \frac{8}{m_{i-1} + m_i}$. To prevent overlap between adjacent kinks, we require that the separation between sub-kinks exceeds their width, *i.e.*, $\xi_{i+1} - \xi_i > \sigma_{k_i}$, leading to the following bound:

$$\alpha < \alpha_1 = 32 \exp\left\{-8 \frac{m_i}{m_i + m_{i+1}}\right\} \approx 0.59. \quad (2.26)$$

Notice that the previous condition is independent of the value of n .

The previous results enable us to construct an approximate expression for the $\Phi_{K_n}(z)$ profile. We assume an ansatz in which the multi-kink is written as a superposition of the sub-kink solutions $\phi_{k_i}(z)$ given in Eq.(2.24) separated by distances given in Eq.(2.24). Hence $\Phi_{K_n}(z)$ takes the following form

$$\Phi_{K_n}(z) = \sum_{i=1}^{\frac{n}{2}} (\phi_{k_i}(z - X_i) + \phi_{k_{-i}}(z + X_i)), \quad (2.27)$$

where the internal kinks are centered at the positions

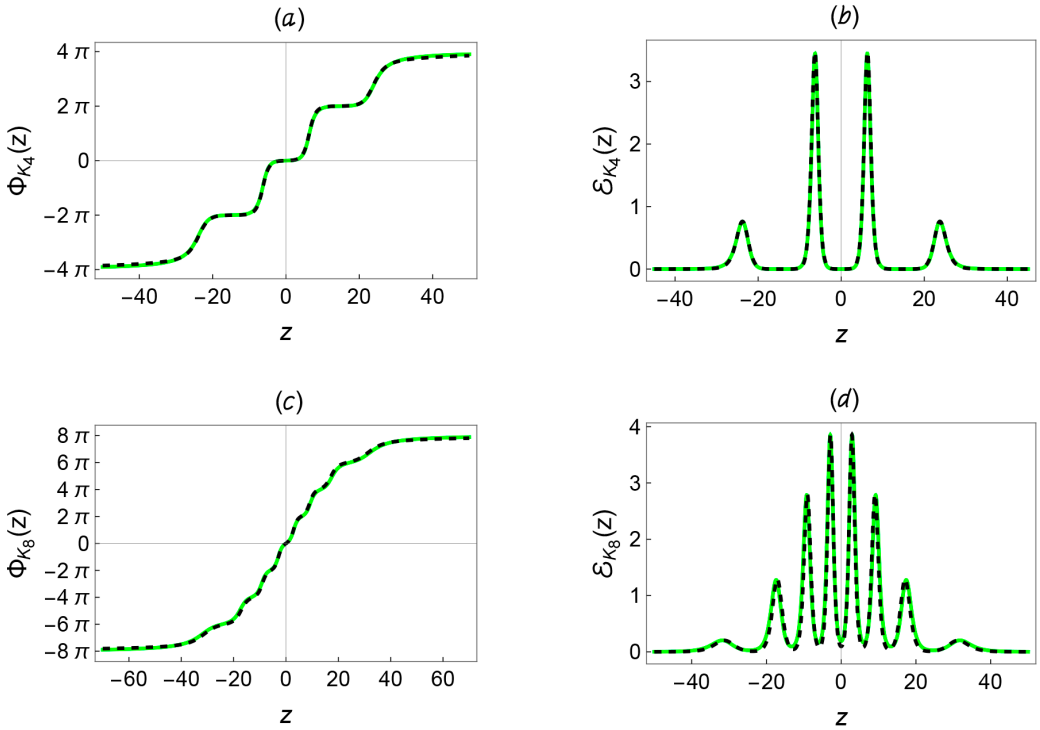


Figure 4. (a) and (c) multi-kinks $\Phi_{K_n}(z)$ obtained from the numerical solution of Eq.(2.5) for the potential $V_{n,\alpha}(\phi)$ in Eq.(2.7) (continuous-green lines) and the analytical ansatz Eq.(2.27) (dashed-black lines). (b) and (d) the corresponding energy density distributions. The parameters values are: $n = 4$, $\alpha = 0.0001$ for the (a) and (b) figures and $n = 8$, $\alpha = 0.1$ in the (c) and (d) cases.

$$X_i = \sum_{j=1}^i \left(1 - \frac{1}{2}\delta_{j,1}\right) (\xi_j - \xi_{j-1}), \quad (2.28)$$

with $\xi_0 \equiv \xi_{-1}$. The multi-kink $\Phi_{K_n}(z)$ is centered at $z = 0$.

Figure (4) compares the multi-kink profile obtained from the numerical solution of the exact Bogomol'nyi equation, Eq.(2.5), with the approximated solution obtained from Eq. (2.27). Importantly, the masses $m_{\pm \frac{n}{2}}$ do not vanish any more, hence, the expression for field $\phi_{k_i}(z)$ in the left side of Eq. (2.15) applies for all values of the indices $i \leq \frac{n}{2}$. The comparison shows excellent agreement between the analytical approximation and the numerical results, with the accuracy improving as α decreases and n increases. The corresponding energy density plot reveals n well-localized energy peaks, each associated with one of the n sub-kinks, confirming the internal structure of the multi-kink configuration.

As established above, K_n is composed of n sub-kinks, and can thus be schematically represented as $K_n \sim \{k_{-\frac{n}{2}}, k_{-\frac{n}{2}+1}, \dots, k_{\frac{n}{2}}\}$.

It is reasonable to assume that the size of an individual sub-kink k_i is characterized by the width of its energy density distribution, given approximately by $\sigma_{k_i} \approx \frac{8}{m_i + m_{i+1}}$. However, the total size of the multi-kink configuration must account for the full extent of

its n internal sub-kinks, as well as half the width of the two outermost sub-kinks, $k_{\pm \frac{n}{2}}$. Accordingly, we define the total multi-kink size $\sigma_{K_{(n,\alpha)}}$ as

$$\sigma_{K_{(n,\alpha)}} = 2 \left(X_{\frac{n}{2}} + \frac{4}{m_{\frac{n}{2}-1} + m_{\frac{n}{2}}} \right), \quad (2.29)$$

where according to Eq.(2.28) $X_{\frac{n}{2}}$ represents the position of the $k_{\frac{n}{2}}$ sub-kink. Figure (3b) displays the multi-kink size as a function of the breaking degeneracy parameter α for various values of n . The result is compared with the approximated expression

$$\sigma_{K_{(n,\alpha)}} \approx \frac{2n}{\pi} \left[\left(\ln \left(\frac{2n}{\pi} \right) + \frac{1}{2} \right) \ln \left(\frac{32}{\alpha} \right) + 4 \right], \quad (2.30)$$

that is worked out considering $\alpha \ll 1$, $n \gg 1$ and using the approximated result $\sum_{j=1}^{\frac{n}{2}-1} \frac{1}{\cos(j\pi/n)} \approx \frac{n}{\pi} \left[\ln \left(\frac{2n}{\pi} \right) + \frac{1}{2} \right]$ in Eqs.(2.25,2.28). Therefore we obtain that the multi-kink size scales as $\sigma_{K_{(n,\alpha)}} \sim \frac{2n}{\pi} \ln(n) \ln(\frac{1}{\alpha})$ as n grows and α decreases, reflecting the enhanced separation between sub-kinks in the weak-coupling regime.

2.5 Sub-kinks and multi-kink spectra

Considering a linear perturbation of the form $\psi(z) = \varphi(z) + \eta(z)e^{i\omega t}$, around a soliton solution $\varphi(z)$, the fluctuation spectrum is obtained from the eigenvalue equation

$$\left[-\frac{d^2}{dz^2} + U_{eff}(z) \right] \eta(z) = \omega^2 \eta(z), \quad (2.31)$$

where the effective potential for the linear excitations is given by $U_{eff}(z) = V_{n,\alpha}(\varphi(z))$. Equation (2.31) was solved numerically for two cases: (i) the $\alpha = 0$ kinks k_i , and (ii) the multi-kink K_n . In both cases, the resulting spectra contain only the translational zero mode and the continuum states, with no evidence of discrete internal (shape) modes.

Although no shape modes are found for the stationary K_n multi-kink configuration, we expect the existence of internal vibrational modes associated with the oscillations of its constituent sub-kinks. To investigate this possibility, we take as the initial configuration an ansatz composed of two contiguous sub-kinks separated by a distance $2a$, given by

$$\varphi_{(i,i+1)}(z, a) = \phi_{k_i}(z + a) + \phi_{k_{i+1}}(z - a) - v_i. \quad (2.32)$$

Equation (2.31) was then solved using the effective potential $U_{(i,i+1)}(z, a) = V_{n,\alpha}(\varphi_{(i,i+1)}(z, a))$. The results for $n = 4$ and $i = 1$ are shown in Fig. (5a), where one observes that the effective potential exhibits a double-well structure, giving rise to two discrete modes. The first corresponds to a quasi-zero mode, whose eigenfunction $\eta_S(a, z)$ is approximately the symmetric combination of the zero modes of k_i and k_{i+1} :

$$\eta_{S,A}(a, z) = \frac{1}{4} \left(\frac{d\phi_{k_i}(z + a)}{dz} \pm \frac{d\phi_{k_{i+1}}(z - a)}{dz} \right), \quad (2.33)$$

in contrast, the antisymmetric combination $\eta_A(a, z)$ represents a genuine discrete mode trapped between the sub-kinks. This interpretation is supported by the results discussed

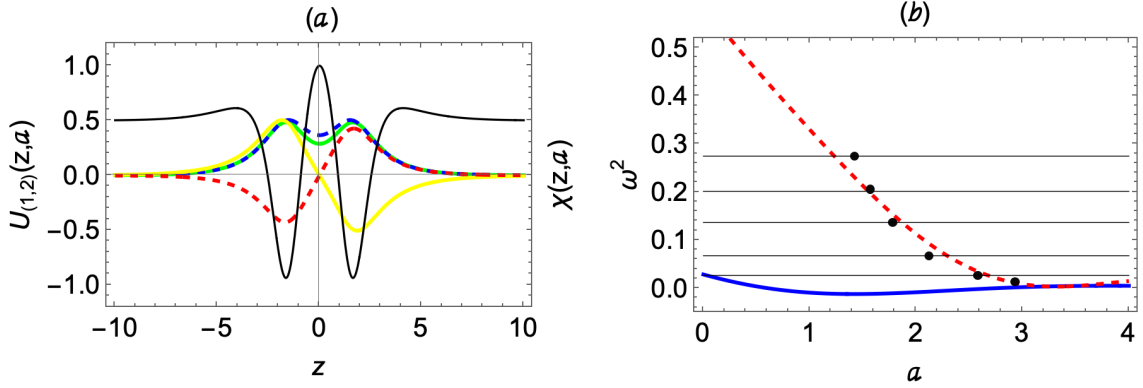


Figure 5. Fluctuation spectra around the $k_1 - k_2$ sub-kink's pair of K_4 . (a) $V_{n,\alpha}(\varphi_{(1,2)}(z, a))$ effective potential (black line) and the $\eta_{S,A}(a, z)$ discrete modes obtained from the solutions of Equation (2.31) (continuous lines) and Equation (2.33) (dashed lines) for $a = 1.6$. (b) Eigenvalues for the symmetric quasi-zero mode (blue solid line) and anti-symmetric (red dashed line) bound states as a function of the sub-kink's separation a . The dots values are obtained from Eqs. (3.7) for α values in the range $\alpha \in \{0.05 - 0.5\}$.

in Section (3.1), where we determine the interaction force $F_{i,i+1}$, Eq. (3.4), acting between neighboring sub-kinks. The predicted values for the equilibrium separation and oscillation frequency, Eqs.(3.5, 3.7), are indicated by the circles in Fig. (5b), showing good agreement with the numerically obtained antisymmetric discrete mode in the small $\alpha \leq 0.5$ regime.

In a collision between the multi-kinks $K_n \equiv \{k_{-\frac{n}{2}}, \dots, k_{\frac{n}{2}}\}$ and $\bar{K}_n \equiv \{\bar{k}_{-\frac{n}{2}}, \dots, \bar{k}_{\frac{n}{2}}\}$, the dynamics is mainly governed by the interaction between the nearest contiguous sub-kinks, namely $k_{\frac{n}{2}}$ and $\bar{k}_{-\frac{n}{2}}$. In this case, the corresponding fluctuation spectrum is obtained by introducing the ansatz

$$\varphi_{(\frac{n}{2}, -\frac{n}{2})}(z, y) = \phi_{k_{\frac{n}{2}}}(z + y) + \phi_{\bar{k}_{-\frac{n}{2}}}(z - y) - v_{\frac{n}{2}}, \quad (2.34)$$

and solving Eq. (2.31) again, now for the effective potential $U_{(\frac{n}{2}, -\frac{n}{2})}(z, y) = V_{n,\alpha}(\varphi_{(\frac{n}{2}, -\frac{n}{2})})$. For this configuration, the effective potential develops a broad central well Fig. (6a), which supports a larger number of internal modes Fig. (6b). The number of such modes increases as the kink-antikink pair separates.

The present analysis indicates that the standard procedure for deriving kink collective coordinate equations of motion [11–14] is impractical here, since no analytical expression exists for the $\Phi_{K_N}(z)$ multi-link or their numerous vibrational shape modes, and those expected in the $K_n - \bar{K}_n$ collision. Instead, we adopt an alternative formulation in which the collective coordinates are described by a set of n nonlinear coupled oscillators. The model is constructed once the inter-sub-kink forces and damping terms due to radiative losses are determined, providing a consistent framework for describing the multi-kink dynamics, as detailed in the following section.

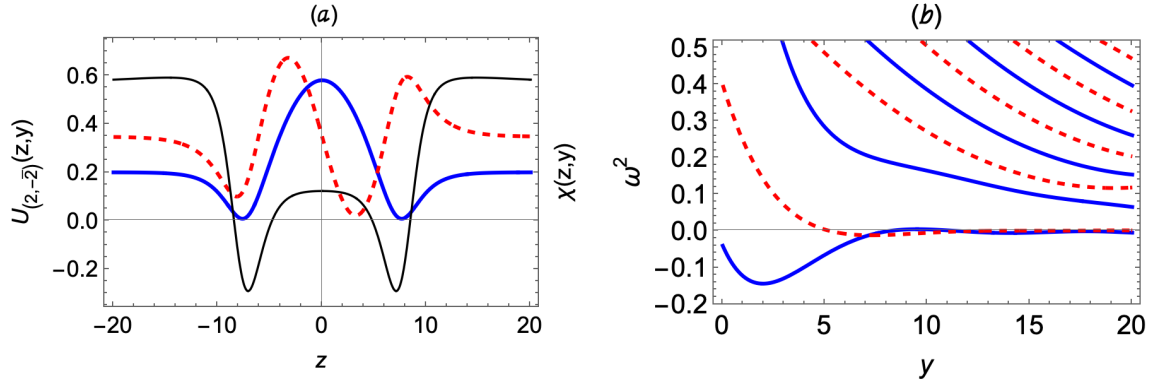


Figure 6. Fluctuation spectra around the $k_2 - \bar{k}_{-2}$ sub-kink's pair in a $K_4 - \bar{K}_4$ collision. (a) $U_{(2,-2)}(z,y)$ effective potential (black line) and the first two discrete modes obtained from the solutions of Equation (2.31) for $y = 7.5$. (b) Even (blue solid line) and odd (red dashed line) bound states eigenvalues as a function of the sub-kink's separation y .

3 Collective coordinate model

We construct a collective coordinate model to describe the dynamics of the multi-kink. Considering that the static ansatz $\Phi_{K_n}(z)$ in Eq.(2.27), obtained by superposing n sub-kinks, provides an accurate approximation to the exact solution, the position X_i of each sub-kink k_i is promoted to a dynamical variable $x_i(t)$. These coordinates evolve according to classical equations of motion under the forces exerted by the adjacent sub-kinks k_{i-1} and k_{i+1} . Approximate expressions for these forces, as well as for the interaction between a K_n multi-kink and its anti-multi-kink, are derived below.

3.1 Forces between $k_i - k_{i+1}$ sub-kinks

Previously, Manton [26] (see also [20]) developed an approach to analyze kink-antikink interactions characterized by long-range power-law tails, rather than the conventional exponential decay. In what follows, we extend this framework to the multi-kink case by introducing an adapted dynamical Bogomol'nyi relation. This generalization enables us to derive the effective forces $F_{i,i+1}$ acting between contiguous sub-kinks ϕ_{k_i} and $\phi_{k_{i+1}}$ that compose a multi-kink configuration K_n . These forces provide the foundation for the collective coordinate model developed in the next section.

Let us assume that the multi-kink configuration $\phi(z)$ satisfies the exact static field equation Eqs.(2.4, 2.5), except in the region $\xi_i \leq z \leq \eta_{i+1}$, where the field $\varphi(z,t)$ departs from the exact $\phi(z)$. Outside this region, the exact field configurations $\phi(z)$ remains intact. The modified field becomes time dependent and is centered at $z = x_{i+1}(t) \equiv x(t)$, thus is written as $\varphi(z - x(t))$, where $x(t)$ represents the position of the sub-kink k_{i+1} . At equilibrium $\varphi(z - x(t))$ is expected to relax to the exact configuration $\phi(z)$ and $x(t) \rightarrow \xi_{i+1}$.

Substituting $\varphi(z - x(t))$, into the time dependent field equation Eq.(2.3) gives

$$\gamma^{-2} \frac{d^2\varphi}{d^2y} - \frac{dV_{n,\alpha}}{d\varphi} + \ddot{x} \frac{d\varphi}{dy} = 0, \quad (3.1)$$

where $y = z - x(t)$ is the argument of φ and $\gamma = 1/\sqrt{1 - \dot{x}^2}$ is the Lorentz contraction factor. Eq.(3.1) can be considered a equation for the field $\varphi(y)$ that evolves adiabatically on time trough its dependence on $x(t)$. In what follows we shall assume that the acceleration \ddot{x} , and the velocity \dot{x} are small, so only leading terms in these quantities will be retained. Multiplying Eq.(3.1) by the term $d\varphi/dy$, and utilizing the relation $d\varphi/dy = dW_{n,\alpha}/d\varphi$ leads to the following expression $\frac{d}{dy} \left(\frac{1}{2} \left(\frac{d\varphi}{dy} \right)^2 - V_{n,\alpha} + \ddot{x} W_{n,\alpha} \right) = 0$, that is easily integrated from an arbitrary value of z to $z = \eta_{i+1}$, where $\varphi(\eta_{i+1}) = v_{i+1}$, to give the following expression

$$\frac{1}{2} \left(\frac{d\varphi}{dy} \right)^2 = [V_{n,\alpha}(\varphi) - \ddot{x} (W_{n,\alpha}(\varphi) - W_{n,\alpha}(v_{i+1}))], \quad (3.2)$$

where we used the fact that φ satisfy the relation $\left[\frac{1}{2} \left(\frac{d\varphi}{dy} \right)^2 - V_{n,\alpha}(\varphi) \right]_{z=\eta_{i+1}} = 0$ Eq.(2.5), at the boundary. Comparing with Eq.(2.5), we observe that Eq.(3.2) can be considered an adiabatic time dependent Bogomol'nyi relation, where the potential $V_{n,\alpha}(\varphi)$ is replaced by an effective potential $V_{eff} = V_{n,\alpha}(\varphi) - \ddot{x} (W_{n,\alpha}(\varphi) - W_{n,\alpha}(v_{i+1}))$.

For a given trajectory $x(t)$, the solution of Eq.(3.2) determines the adiabatic evolution of the field φ . Additionally, an integration of this equation throws an expression for the evolution of the coordinate $x(t)$. The limits are selected from $z = \xi_i$ where $\varphi = \Omega_i$, to $z = x(t)$ with $\varphi(x(t)) \rightarrow \Omega_{i+1}$, to obtain

$$\int_{\Omega_i}^{\Omega_{i+1}} \frac{d\varphi}{\sqrt{2[V_{n,\alpha}(\varphi) + \ddot{x} (W_{n,\alpha}(v_{i+1}) - W_{n,\alpha}(\varphi))]} = x(t) - \xi_i. \quad (3.3)$$

This equation represents an implicit relation between the kink acceleration \ddot{x} and $x(t)$, that is the effective equation of motion for the coordinate $x(t)$. In particular, equilibrium is reached when $\ddot{x} \rightarrow 0$ and $x(t) \rightarrow \xi_{i+1}$, reducing to the correct expression for the separation between the contiguous k_i and k_{i+1} kinks given in Eq.(2.23).

Approximated analytical expressions for the equation of motion for $x(t)$ and the equilibrium separation $\xi_{i+1} - \xi_i$ can be obtained from Eq.(3.3). The leading contribution to the integral in Eq.(3.3) arises from values of φ in the region close to the potential minimum $\varphi \sim v_i$. Hence we expand the potential $V_{n,\alpha}(\varphi) = V_{n,0}(\varphi) + \alpha \Delta_{n,\alpha}(\varphi) \approx \frac{1}{2} m_i^2 (\phi - v_i)^2 + \alpha \Delta_{n,\alpha}(v_i)$, where $m_i^2 = (d^2 V_{n,\alpha} / d^2 \phi)_{\phi=v_i}$ is the mass of the perturbative scalar oscillations around v_i , and we verify that to leading order $W_{n,\alpha}(\varphi) \approx W_{n,\alpha}(v_i)$. The resulting expression is readily integrated, and identifying the k_i kink mass $M_{k_{i+1}} = W_{n,\alpha}(v_{i+1}) - W_{n,\alpha}(v_i)$, the relation between \ddot{x} and x takes the form of a Newton equation of motion,

$$M_{k_{i+1}} \ddot{x}_{i+1} = F_{\{i,i+1\}}(\xi_i, x_{i+1}) = 2m_i^2 [(\Omega_{i+1} - v_i)(v_i - \Omega_i)] e^{-m_i(x_{i+1} - \xi_i)} - \alpha \Delta_{n,\alpha}(v_i). \quad (3.4)$$

The first contribution corresponds to the repulsive force that typically acts between kinks, while an additional attractive term arises from the negative pressure exerted by the false-vacuum region trapped between the kink's pair. At equilibrium, $x(t) \rightarrow \xi_{i+1}$, and the condition of vanishing total force determines the equilibrium separation as

$$\delta\xi_{\{i,i+1\}} = \xi_{i+1} - \xi_i = \frac{1}{m_i} \ln \left[\frac{2(\Omega_{i+1} - v_i)(v_i - \Omega_i)}{\alpha} \right], \quad (3.5)$$

where, to leading order in α , we take into account that $\Delta_{n,\alpha}(v_i) \approx m_i^2$. The potential energy associated to $F_{\{i,i+1\}}$ is given as

$$U_{\{i,i+1\}}(x_{i+1} - x_i) = \alpha m_i \left[e^{-m_i[y - \delta\xi_{\{i,i+1\}}]} - 1 + m_i(y - \delta\xi_{\{i,i+1\}}) \right]_{y=x_{i+1}-x_i}. \quad (3.6)$$

For small oscillations of the sub-kinks around their equilibrium separations, these results allow us to determine the corresponding oscillation frequency as

$$\omega_{i,i+1} = \sqrt{\frac{\alpha m_i^3}{\mu_{i,i+1}}}, \quad \mu_{i,i+1} = \frac{M_{k_i} M_{k_{i+1}}}{M_{k_i} + M_{k_{i+1}}}. \quad (3.7)$$

The previous results also apply for negative values of the indices, with the replacement $F_{-(i+1),-i}(a) \rightarrow -F_{i,i+1}(a)$. This extension includes the case of $F_{-1,1}(a)$, taking into account that $v_0 = 0$, $\Omega_{-1} = -\Omega_1$ and $m_0 = 1$. In particular, the equilibrium separation and the corresponding oscillation frequency reduce to

$$\delta\xi_{\{-1,1\}} = \xi_1 - \xi_{-1} = \ln \left[\frac{2\Omega_1^2}{\alpha} \right], \quad \omega_{-1,1} = \sqrt{\frac{2\alpha}{M_1}}. \quad (3.8)$$

The predicted values for $\delta\xi_{\{1,2\}}$ and $\omega_{1,2}$ in Eqs.(3.5, 3.7) are compared with the results obtained from the fluctuation spectra obtained from the solution of Eq.(2.31) in Figure 5, showing a good agreement in the $\alpha \leq 0.5$ regime.

3.2 Force between K_n and \bar{K}_n multi-kinks

As previously mentioned the collision between the multi-kinks K_n and \bar{K}_n is dominated by the interaction between the nearest contiguous sub-kinks. To determine the $k_{\frac{n}{2}} - \bar{k}_{-\frac{n}{2}}$ interaction we consider the ansatz given in Eq.(2.34). However, the method used in the previous section does not apply in the present situation, since the field configurations do not possess equilibrium positions that would allow us to define the integration limits required in Eq. (3.3). Instead, we consider the force exerted by the field in the $z < 0$ region upon the one occupying the $z > 0$ region, which can be expressed as follows [1]:

$$F(y) = \left[\frac{1}{2} \left(\frac{d\varphi(z, y)}{dz} \right)^2 - V_{n,\alpha}(\varphi(z, y)) \right]_{z=0}. \quad (3.9)$$

Substituting in this equation the ansatz (2.34) and considering the limit $y \gg 1$, leads to the following approximate form for the interaction force

$$F_{k_{\frac{n}{2}}, \bar{k}_{-\frac{n}{2}}}(y) = -C_{n,\alpha} e^{-4m_{\frac{n}{2}}y}, \quad C_{n,\alpha} = \frac{512}{n^2} \left[b_{\frac{n}{2}} \right]^4. \quad (3.10)$$

This corresponds to the well-known attractive kink-antikink interaction, which provides a reliable description for large separations $y \gg 1$. However, for small separations $y \sim 0$, it leads to an unphysical kink-antikink penetration that is not observed in field-theory collision studies. Several solutions have been proposed in the literature to overcome this issue [11–14], but a simple phenomenological prescription [44] is to introduce a short-range repulsive core. This prevents the unphysical penetration and ensures that the $y \rightarrow -y$ symmetry is preserved throughout the entire evolution. Accordingly, we propose to replace Eq. (3.10) by a Morse-type interaction

$$F_{k_{\frac{n}{2}}, \bar{k}_{-\frac{n}{2}}}(y) = \lambda C_{n,\alpha} \left(e^{-8m_{\frac{n}{2}}y} - e^{-4m_{\frac{n}{2}}y} \right), \quad (3.11)$$

where λ is an undetermined parameter of the interaction, that will be fixed comparing the results of the collective coordinate model results with those obtained from the field calculation at one particular point on the parameters space. With the addition of the repulsive core, we have a confining interaction with an small oscillation frequency give as

$$\omega_{k_{\frac{n}{2}}, \bar{k}_{-\frac{n}{2}}} = \sqrt{\frac{4\lambda C_{n,\alpha} m_{\frac{n}{2}}}{M_{k_{\frac{n}{2}}}}}, \quad (3.12)$$

and the potential energy is given as.

$$U_{k_{\frac{n}{2}}, \bar{k}_{-\frac{n}{2}}}(y) = \frac{\lambda C_{n,\alpha}}{4m_{\frac{n}{2}}} \left(\frac{1}{2} e^{-8m_{\frac{n}{2}}y} - e^{-4m_{\frac{n}{2}}y} \right). \quad (3.13)$$

3.3 Radiation energy losses

In previous investigations, kink radiation has been attributed to the decay of a single shape mode whose oscillation frequency lies below the scalar mass threshold. Consequently, it can only arises as a nonlinear effect that proceeds through a second- or higher-harmonic mechanism [39, 45–47]. In contrast, the $K_n - \bar{K}_n$ collision spectra displays an ample range of characteristics frequencies ω_l . Although many of these frequencies lie below the scalar mass thresholds $\omega_l < m_i$, there is a significant number of frequencies located above the $m_{\frac{n}{2}}$ threshold that contribute to the radiative energy losses. This feature makes it possible to establish a first-order perturbative scheme in which back-reaction radiation effects are incorporated into an effective force that modulates the dynamical evolution of the collective coordinates $x_i(t)$.

Suppose we consider the field $\varphi(t, z) = \phi_{k_i}(z - x_i(t)) + f_i(t, z)$, where $f_i(t, z)$ denotes the radiation field emitted by the i -th sub-kink and $\phi_{k_i}(z)$ is the kink-solution in the $\alpha = 0$ limit. Substituting this ansatz into the field equation of motion Eq. (2.3), and expanding to leading order in $f_i(t, z)$, we obtain

$$\left(\frac{\partial^2}{\partial t^2} - \frac{\partial^2}{\partial z^2} - m_i^2 \right) f_i(t, z) = \ddot{x}_i \frac{\partial \phi_{k_i}}{\partial \xi}, \quad (3.14)$$

where we neglected terms of order \dot{x}_i^2 and $\alpha \frac{\partial \Delta V_{n,\alpha}}{\partial \phi}$, and approximate

$$\frac{\partial^2 V_{n,\alpha}[\phi_{k_i}(\xi)]}{\partial \phi^2} \approx m_i^2. \quad (3.15)$$

Henceforth we denote $v_i = \dot{x}_i$ and $a_i = \ddot{x}_i$. The solution can then be obtained using the one-dimensional Klein-Gordon Green's function, which yields [5, 48]

$$f_i(t, z) = \frac{1}{2} \int_{t_1} dt' \int dz' \Theta(t - t' - |z - z'|) J_0 \left(m_i \sqrt{(t - t')^2 - (z - z')^2} \right) a_i(t') \frac{\partial \phi_{k_i}}{\partial \xi'}, \quad (3.16)$$

where $\xi' = z' - x_i(t')$, Θ denotes the Heaviside step function, and J_0 is the Bessel function of the first kind. The last term in this equation is strongly localized around the sub-kink position and can therefore be approximated as $\frac{\partial \phi_{k_i}(z' - x_i(t'))}{\partial \xi'} \approx 2\pi \delta_D(z' - x_i(t'))$, where δ_D is the Dirac delta. Under this approximation, Eq.(3.16) simplifies to

$$f_i(t, z) = \pi \int_{t_1} dt' \Theta(t - t' - |z - x_i(t')|) J_0 \left(m_i \sqrt{(t - t')^2 - (z - x_i(t'))^2} \right) a_i(t'). \quad (3.17)$$

The radiated energy per unit time is obtained from the Poynting term

$$S_i[t, z_R] = \left[\frac{\partial f_i}{\partial t} \frac{\partial f_i}{\partial z} \right]_{z=z_R}, \quad (3.18)$$

where z_R is an observation point located at the radiation region $z_R > x_i$. Differentiating the radiation field with respect to t and z , and assuming that $z \gg x_i$, one finds

$$\begin{aligned} \frac{\partial f_i}{\partial t} &= \pi a_i(t - z) - \pi m_i \int_{t_1}^{t-z} dt' \frac{m_i(t - t')}{\sqrt{(t - t')^2 - z^2}} J_1 \left(m_i \sqrt{(t - t')^2 - z^2} \right) a_i(t'), \quad (3.19) \\ \frac{\partial f_i}{\partial z} &= -\pi a_i(t - z) + \pi m_i \int_{t_1}^{t-z} dt' \frac{m_i z}{\sqrt{(t - t')^2 - z^2}} J_1 \left(m_i \sqrt{(t - t')^2 - z^2} \right) a_i(t'). \end{aligned}$$

As previously discussed, the acceleration spectra $a_i(\omega)$ are expected to contain a broad range of frequencies. In contrast, the field-radiation spectra $f_i(\omega, z_R)$ should include only propagating modes with $\omega > m_i$. This implies that the Bessel functions appearing in Eqs. (3.17) and (3.19) effectively act as frequency filters. This interpretation is fully consistent with the numerical results presented in section(3.4), as shown in Figures (9).

For the internal sub-kinks involved in a K_n - \bar{K}_n collision, Fig. (8a) shows that shortly after the collision their acceleration spectra display a broad set of characteristic frequencies. Nonetheless, two sharply contrasting patterns emerge. For the internal sub-kinks, virtually all frequency modes lie below the corresponding mass threshold m_i , whereas the external sub-kink exhibits a significant fraction of modes above the radiation threshold. Consistent with this behavior, the $f_i(\omega)$ spectra in Fig. (9) shows a strong radiation suppression for the internal sub-kinks, while nearly all radiation originates from the external sub-kinks.

A complete treatment of these effects would require solving a complicated system of coupled nonlinear integro-differential equations, which lies beyond the scope of the present work. However, the previous results motivate a simple self-consistent approximation that can be implemented by proposing the relations

$$\left[\frac{\partial f_i(t)}{\partial t} \right]_{ap} \approx \pi \sqrt{\beta_i(t)} a_i(t), \quad \left[\frac{\partial f_i(t)}{\partial z} \right]_{ap} \approx -\pi \sqrt{\beta_i(t)} a_i(t). \quad (3.20)$$

Here $\beta_i(t)$ is a slow varying time-dependent function introduced to ensure that, on average, the total radiated power is incorporated correctly. The function $\beta_i(t)$ is therefore determined by requiring that, over successive time intervals, the radiation energy losses computed from Eqs. (3.19) and (3.20) remains mutually consistent

$$\int_0^{\omega_{\max}} \left[\frac{\partial f_i}{\partial t}(\omega) \right] \left[\frac{\partial f_i}{\partial z}(\omega) \right] d\omega \sim \int_0^{\omega_{\max}} \left[\frac{\partial f_i}{\partial t}(\omega) \right]_{ap} \left[\frac{\partial f_i}{\partial z}(\omega) \right]_{ap} d\omega. \quad (3.21)$$

Under this approximation, the Poynting term in Eqs. (3.18) reduces to the simple expression

$$S_i[t] = -\pi^2 \beta_i(t) a_i(t)^2. \quad (3.22)$$

This result allows us to obtain an explicit expression for the back-reaction force $F_{\text{rad},i}$ by requiring that the work done by this force matches the radiated energy loss over the same time interval. This results in an Abraham-Lorentz type expression

$$F_{\text{rad},i} = \pi^2 \left(\beta_i \frac{da_i}{dt} + a_i \frac{d\beta_i}{dt} \right). \quad (3.23)$$

The first term corresponds to the effective damping acting on the i -th sub-kink, while the second term yields a correction to its effective mass.

3.4 Equations of motion

Finally, collecting the previous results we can establish the collective coordinate model that describes the $K_n - \bar{K}_n$ collisions. From now on, we consider the $n = 4$ case, its extension to arbitrary n is straightforward. The equations of motion govern the evolution of the sub-kink components of $\bar{K}_4 \sim \{\bar{k}_{-2}, \bar{k}_{-1}, \bar{k}_1, \bar{k}_2\}$, while the corresponding components of K_4 are obtained by imposing the $z \rightarrow -z$ symmetry.

In this model, only interactions between a sub-kink and its nearest neighbors are taken into account. Consequently, the equations of motion take the following form

$$M_{k_i} \ddot{x}_i = \mathcal{F}_i(x_{i-1}, x_i, x_{i+1}), \quad i = -2, -1, 1, 2, \quad (3.24)$$

where \mathcal{F}_i is constructed using Eqs.(3.4,3.11) and leads to:

$$\begin{aligned} \mathcal{F}_{-2}(x_{-2}, x_{-1}) &= F_{\{K_2 - \bar{K}_2\}}(x_{-2}) + F_{\{1,2\}}(x_{-1} - x_{-2}), \\ \mathcal{F}_{-1}(x_{-2}, x_{-1}, x_1) &= -F_{\{1,2\}}(x_{-1} - x_{-2}) - F_{\{-1,1\}}(x_1 - x_{-1}), \\ \mathcal{F}_1(x_{-1}, x_1, x_2) &= F_{\{-1,1\}}(x_1 - x_{-1}) - F_{\{1,2\}}(x_2 - x_1), \\ \mathcal{F}_2(x_1, x_2) &= F_{\{1,2\}}(x_2 - x_1). \end{aligned} \quad (3.25)$$

It is straightforward to verify that the equations of motion, Eqs.(3.24,3.25), follow from the Euler-Lagrange equations applied to the Lagrangian function $L[x_i, \dot{x}_i] = T - U[x_i]$, where the kinetic energy and potential terms are given as follows:

$$T = \sum_{i=-2, i \neq 0}^{i=2} \frac{1}{2} M_{k_i} \dot{x}_i^2, \quad (3.26)$$

$$U[x_i] = U_{K_n, \bar{K}_n}(x_{-2}) + U_{\{1,2\}}(x_{-1} - x_{-2}) + U_{\{-1,1\}}(x_1 - x_{-1}) + U_{\{1,2\}}(x_2 - x_1),$$

where the interaction potential $U_{\{i,i+1\}}$ and U_{K_n, \bar{K}_n} are defined in Eqs.(3.6,3.13). These results allow us to verify that, to a high degree of precision, the numerical solutions of the equations of motion Eq.(3.24) are consistent with the conservation of the total energy $E_{CCM} = T + U$.

Back-radiation effects on the sub-kinks can be incorporated by adding the force term $F_{\text{rad},i}$ from Eq. (3.23) to the equations of motion. However, a direct substitution of terms involving the time derivative of the acceleration leads to the well-known issue of runaway solutions. To avoid this, we adopt the perturbative method of Landau and Lifshitz, in which the first-order solution of $M_{k_i} \ddot{x}_i = \mathcal{F}_i$ is used to evaluate the acceleration time derivative term appearing in Eq.(3.23) and thereby estimate $F_{\{rad,i\}}$. Taking these considerations into account, the equations of motion take the following form:

$$\tilde{M}_{k_i} \ddot{x}_i = \mathcal{F}_i(x_{i-1}, x_i, x_{i+1}) + \pi^2 \frac{\beta_i(t)}{M_{k_i}} \sum_j (v_j - v_i) \left[\frac{\partial \mathcal{F}_j(\xi)}{\partial \xi} \right]_{\xi=(x_j - x_i)}, \quad (3.27)$$

where $\tilde{M}_{k_i} = M_{k_i} - \pi^2 \frac{d\beta_i}{dt}$. With the inclusion of radiative effects, the total particle energy $E_{CCM} = T + U$ is no longer conserved. However, one can verify that the energy loss ΔE_{CCM} over a given time interval is consistent with the radiated energy obtained from the time integral of the Poynting term

$$E_{CCM}(t_2) - E_{CCM}(t_1) \approx E_{\text{rad}}(t_1, t_2) = \sum_i \int_{t_1}^{t_2} \beta_i(t) S_i[t, z_R] dt. \quad (3.28)$$

A consistent solution of Eqs. (3.27) requires knowledge of the function $\beta_i(t)$. To determine it, we employ a recursive approximation scheme. In the first step, we set $\beta_i \equiv 0$ and solve the equations of motion (3.24). Once the trajectories $x_i(t)$ and their time derivatives are obtained, all quantities entering Eqs. (3.17), (3.18), and (3.19), as well as the required Fourier transforms, can be evaluated. Then, for a sequence of post-collision time intervals $t_{pc} \in \{t_{pc} - \delta t, t_{pc} + \delta t\}$, values of $\beta_i(t_{pc})$ are determined from Eq. (3.21). Two or three iterations of the process, solving Eqs. (3.27), leads to convergent results, *e.g.* for $\alpha = 0.05$ and $v_i = -0.1$:

$$\begin{aligned} \beta_i(t) &\approx \frac{\tilde{\beta}_i}{\pi} \left(\arctan \left[-m_{\text{eff}} \left(t - \left(\frac{X_L}{|v_i|} + t_c \right) \right) \right] + \frac{\pi}{2} \right), \quad m_{\text{eff}} \approx 0.0002, \quad t_c \approx 6400, \\ \tilde{\beta}_{-2} &\approx 0.017, \quad \tilde{\beta}_{-1} \approx 0.0018, \quad \tilde{\beta}_1 \approx 0.08, \quad \tilde{\beta}_2 \approx 0.9. \end{aligned} \quad (3.29)$$

The extracted $\tilde{\beta}_i$ values confirm that radiation is strongly suppressed for internal sub-kinks and originates primarily from the external one. The time dependence of $\beta_i(t)$ captures the early energy loss during the first rebounds, followed by stabilization into a long-lived oscillon. Although obtained for a particular selection of α and v_i , the results in Eqs. (3.29) vary only weakly within the ranges $\alpha \in [0.01, 0.5]$ and $v_i \in [-0.01, -0.5]$.

The (x_i, \dot{x}_i) phase-space portrait for a solution of Eqs. (3.27) is shown in Fig. (7a). The evolution spans a long interval, $t \in [0, 190, 000]$, and is consistent with the formation

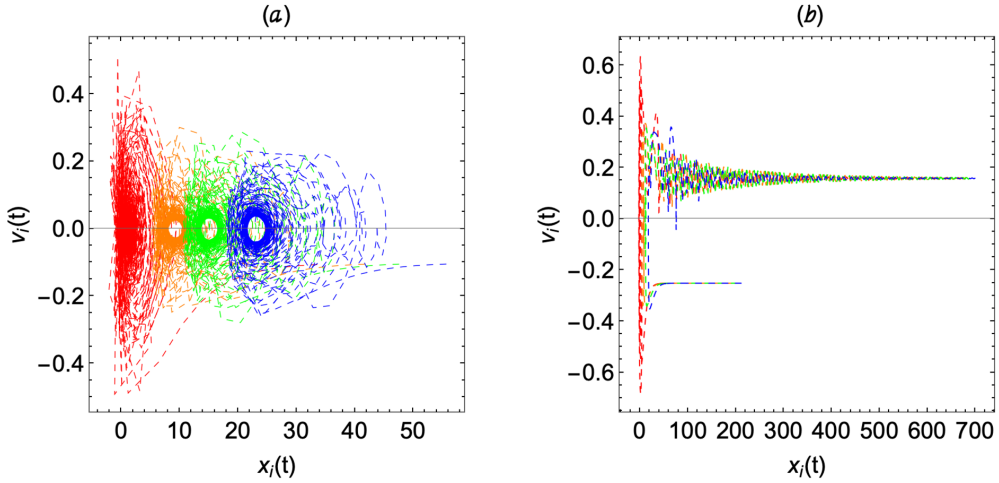


Figure 7. The (x_i, \dot{x}_i) phase space portrait for $K_4 - \bar{K}_4$ collision solutions of Eqs. (3.27). The trajectories correspond to the: \bar{k}_{-2} (red line), \bar{k}_{-1} (orange line), \bar{k}_1 (green line), and \bar{k}_2 (blue line) sub-kinks. (a) Oscillon evolution in the $t \in \{1500, 100000\}$ time interval, for $v_{in} = -0.1$. (b) Inelastic dispersion for $t \in \{0, 15000\}$, when $v_{in} = -0.25$. Here $n = 4$, $\alpha = 0.05$, and $\lambda = 0.1$.

of a long-lived oscillon: the oscillation amplitude decreases significantly during the first rebounds, and for $t > 10,000$ the (x_i, \dot{x}_i) trajectories settle around slowly contracting elliptic limit cycles, as expected for a metastable configuration with weak radiative damping. A detailed comparison with the corresponding full field simulation will be presented in the next section. The energy balance also confirms the consistency of the collective coordinate model, with $E_{CCM}(20000) - E_{CCM}(0) = -0.8905$ and $E_{rad}(0, 20000) = -0.8946$, showing excellent agreement with Eq. (3.28).

Figure (8a) shows the acceleration spectra $a_i(\omega)$, evaluated shortly after the first rebound for each of the four sub-kinks, together with their respective radiation thresholds m_i . As anticipated, the spectra contain a large set of resonant frequencies, yet only those associated with the external sub-kink lie above the radiation threshold. In contrast, Figure (8b) shows that once the system settles into its quasi-stable stage, the acceleration spectrum is drastically reduced, exhibiting only a few dominant frequency peaks. Figure (9a) displays the total radiation field $f_T(t, z_R)$ in the radiation region $z_R > x_i$, whereas the $f_i(\omega)$ Fourier spectra corroborates that only the external sub-kink k_2 contributes significantly to radiation energy losses.

For a higher incident speed, $v_{in} = -0.25$, the phase-space trajectories (x_i, \dot{x}_i) shown in Fig. (7b) correspond to an inelastic collision in which the multi-kink rebounds with a final velocity $v_{fin} \simeq 0.16$. In this case we have $E_{CCM}(90000) - E_{CCM}(0) = -0.39$ and $E_{rad}(0, 90000) = -0.43$.

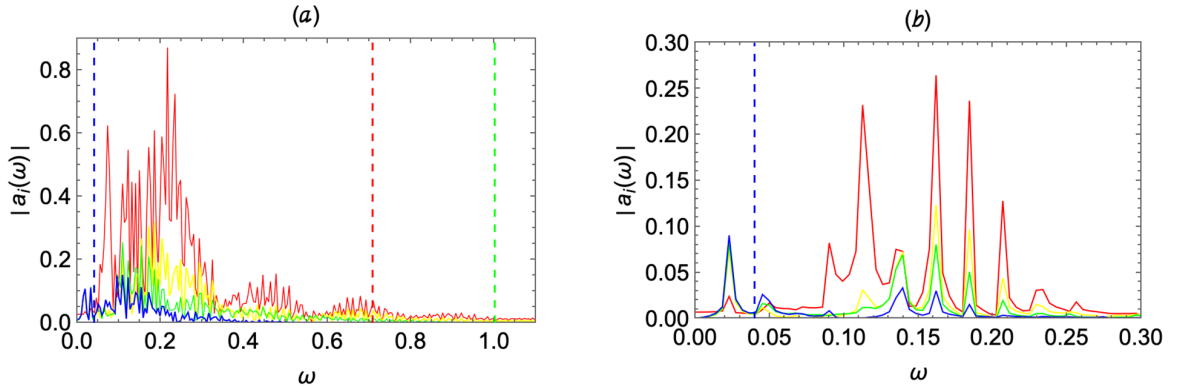


Figure 8. Acceleration spectra for the sub-kinks: \bar{k}_{-2} (red), \bar{k}_{-1} (yellow), \bar{k}_1 (green), and \bar{k}_2 (blue), in a $K_4 - \bar{K}_4$ collision, and its corresponding m_i radiation thresholds (vertical lines). (a) Evaluated at $t = 2000$, just after the first rebound. (b) At $t = 10000$, when the system has reached a quasi-stable stage. The parameters are selected as: $n = 4$, $\alpha = 0.05$, $\lambda = 0.1$, and $v_{in} = -0.1$.

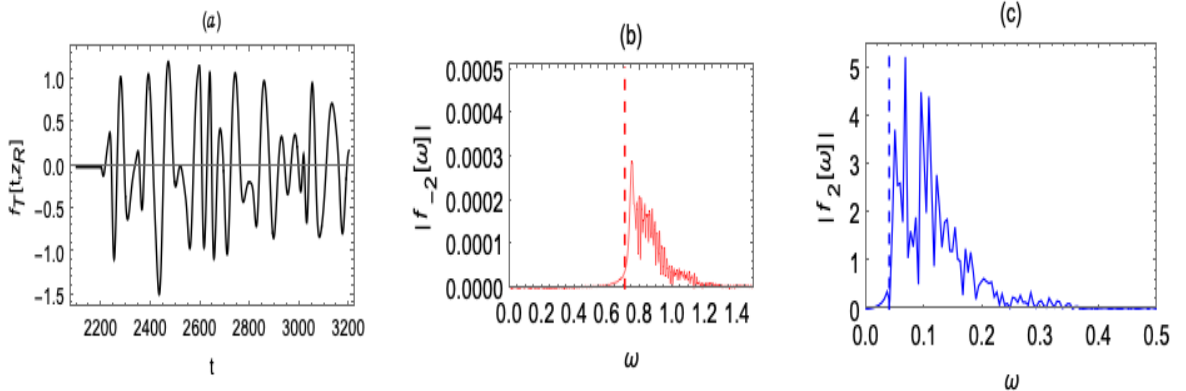


Figure 9. (a) Total field radiation $f_T(t, z_R)$ obtained from the sum of the sub-kink contributions in Eq. (3.17). Field $f_i(\omega, z_R)$ spectra for the: (b) k_{-2} (red), and (c) k_2 (blue) sub-kinks, evaluated after the first rebound, $t = 2000$, and its corresponding m_i radiation thresholds (vertical lines). The parameters are selected as $n = 4$, $\alpha = 0.05$, $\lambda = 0.1$, $v_{in} = -0.1$, and $z_r = 400$.

4 Multi-kink collisions

We study the collisions between two multi-kinks by numerically solving Eq. (2.3) with the initial ansatz

$$\Phi_{K_4 K'_4}(z) = \Phi_{K_4}(z + X_L - v_{in} t) + \Phi'_{K_4}(z - X_L + v_{in} t) - 4\pi, \quad (4.1)$$

which represents a head-on collision between two $n = 4$ multi-kinks. The simulations employ a temporal step $\tau \approx 0.12$ and a spatial grid with spacing $h \approx 0.41$, comprising 12,000 points over $z \in [-2500, 2500]$. Absorbing boundaries are placed sufficiently far from the interaction region to prevent reflections. Initial multi-kink profiles are computed using

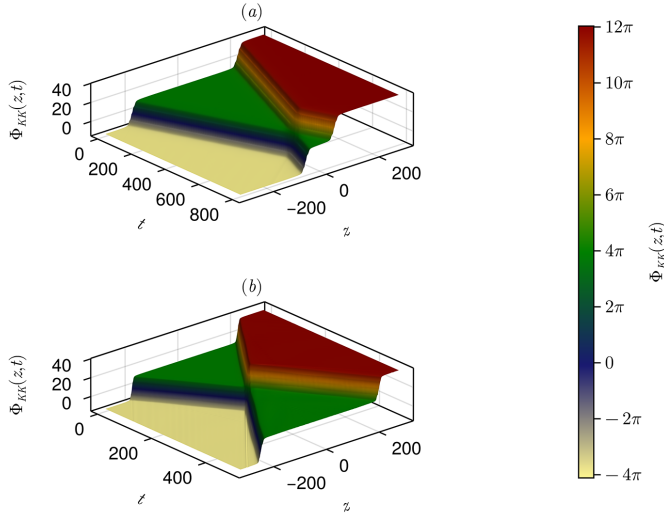


Figure 10. Space-time picture for the collision of two $n = 4$ contiguous multi-kinks $K\{-4\pi, 4\pi\}_{v_{in}} + K\{4\pi, 12\pi\}_{-v_{in}} \rightarrow K\{-4\pi, 4\pi\}_{-v_{fi}} + K\{4\pi, 12\pi\}_{v_{fi}}$. The initial velocities are: (a) $v_{in} = -0.2$ and (b) $v_{in} = -0.9$, the other parameters are selected as $L = 200$ and $\alpha = 0.05$.

a fourth-order Runge-Kutta scheme. We consider the case $n = 4$ with an initial separation $X_L = 200$. Since the multi-kink size satisfies $\sigma_{K_4} \leq 50$ (see Fig. 3b), this choice guarantees negligible initial overlap between the colliding configurations. Throughout this section, the notation $K\{v_i, , v_i + 2n\pi\}$ is used to denote the vacuum sector in which a given multi-kink is defined.

4.1 $K_n - K_n$ collisions

We first examine the collision between two contiguous $n = 4$ multi-kinks: $K\{-4\pi, 4\pi\}_{v_{in}} + K\{4\pi, 12\pi\}_{-v_{in}} \rightarrow K\{-4\pi, 4\pi\}_{-v_{fi}} + K\{4\pi, 12\pi\}_{v_{fi}}$. The total topological charge $Q_{2 \times 4} = 8$ is conserved, ensuring that the field always interpolates between $\phi \rightarrow -4\pi$ and $\phi \rightarrow 12\pi$ at spatial infinities.

As shown in Fig. (10), the internal structure of each multi-kink is largely preserved for a broad range of velocities, including $v_{in} = -0.2$ and $v_{in} = -0.9$. After the collision, both multi-kinks rebound and recover their initial profiles, moving apart with final velocities v_{fi} . The process resembles the elastic two-soliton collisions of the sine-Gordon model, though here it is inelastic: small internal oscillations and weak radiation losses appear, yet the integrity of the multi-kink structure is preserved.

4.2 $K_n - \bar{K}_n$ collisions

We investigate the collision between a $K\{-4\pi, 4\pi\}$ multi-kink and its corresponding anti-multi-kink $\bar{K}\{4\pi, -4\pi\}$. Because the total topological charge of this configuration is zero, the dynamics can lead to three distinct outcomes Fig. 11: (a) the formation of a long-lived

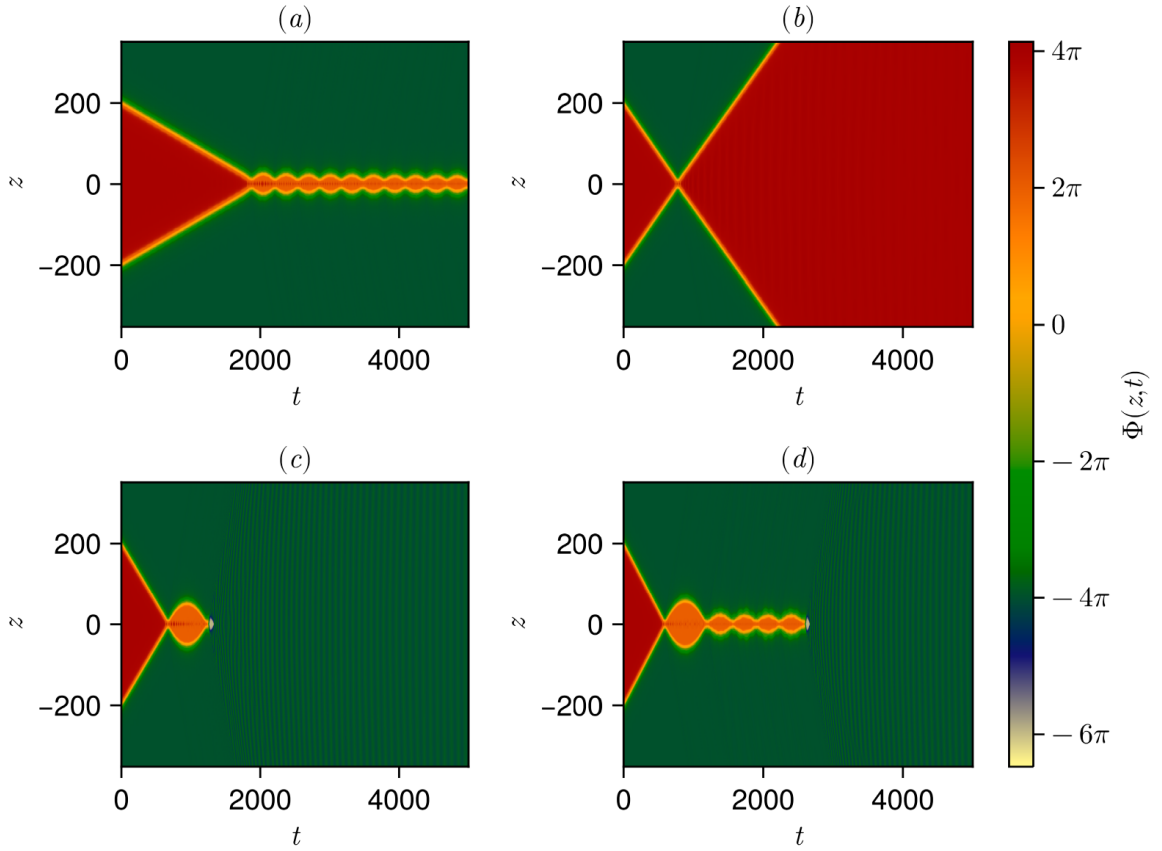


Figure 11. Space-time plots of the $K_4 - \bar{K}_4$ collisions with various initial velocities: (a) $v_{in} = -0.1$, (b) $v_{in} = -0.25$, (c) $v_{in} = -0.29$, and (d) $v_{in} = -0.332$. In all cases $L = 200$, $n = 4$ and $\alpha = 0.05$.

bound state, (b) an inelastic scattering process in which the multi-kinks separate after a single bounce, and (c,d) complete $K_4 - \bar{K}_4$ annihilation into the $v_i = -4\pi$ vacuum.

The final state depends on the parameters α and v_{in} , as illustrated by the α - v_{in} plot of $\Phi_{K\bar{K}}(0, T)$. For $\alpha < \alpha_c \simeq 0.15$, low-velocity collisions tend to produce long-lived bound states, whereas higher incoming velocities lead to either dispersion or annihilation. In contrast, for $\alpha > \alpha_c$ the dynamics are dominated by annihilation events. The boundaries between these regimes exhibit a highly interlaced structure, featuring transition layers and isolated islands.

Figure (13) presents a sequence of snapshots illustrating the time evolution of the bound state that emerges after the $K_4 - \bar{K}_4$ collision. The resulting configuration can be interpreted as a composite large amplitude oscillon: its outer regions retain the structure of the original multi-kinks, while the central zone originates from the fusion of the innermost k_2 - \bar{k}_2 sub-kinks, forming a localized bion oscillating around the false vacuum at $v = 2\pi$. The bion remains linked to the outer segments of the oscillon through the binding force given in Eq. (3.4).

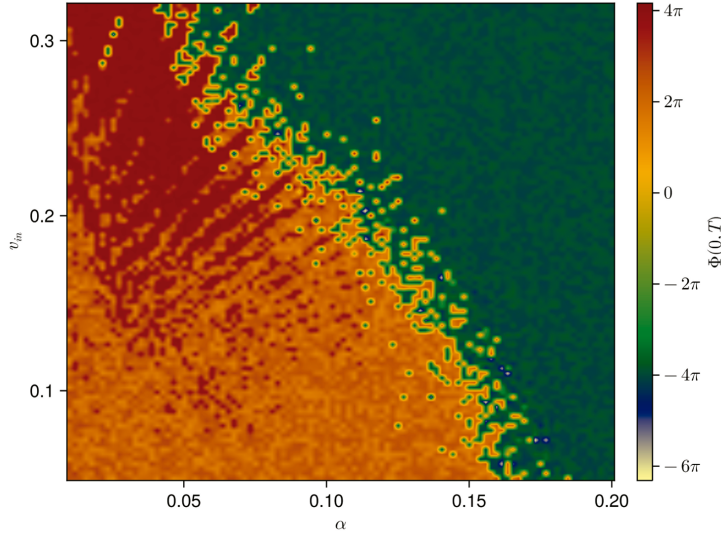


Figure 12. Field configuration $\Phi_{K\bar{K}}(0, T)$ for the $K_4 - \bar{K}_4$ collision, evaluated at the centre of the collision ($z = 0$) at a large time $T \approx 3000$, as a function of the initial speed $|v_{in}|$ and the α breaking degeneracy parameter. T is measured once the initial trajectories intersect.

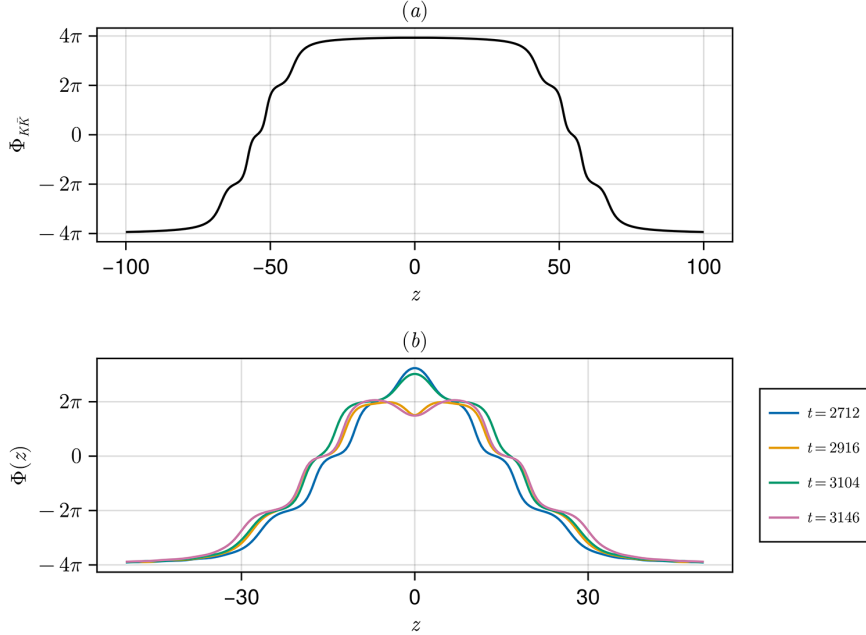


Figure 13. (a) Field configuration before the $K_4 - \bar{K}_4$ collision. (b) Post-collision field snapshots at various times. The configuration can be identified with a composite oscillon that maintains part of the colliding multi-kinks structure, but its central region corresponds to a bion that results from the merging of k_2 and \bar{k}_{-2} sub-kinks. The parameters values are $\alpha = 0.05$, $n = 4$, $L = 200$ and $v_{in} = -0.1$.

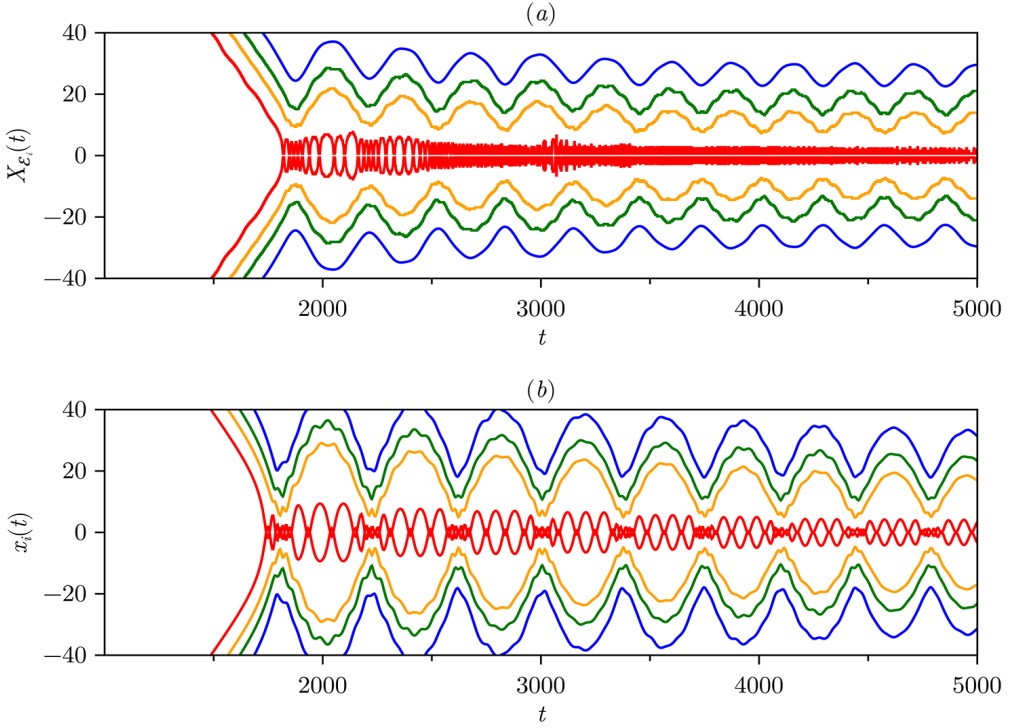


Figure 14. Oscillon evolution shortly after the $K_4 - \bar{K}_4$ collision, according the: (a) Full field or (b) collective coordinates description. The parameters values are $\alpha = 0.05$, $n = 4$, $L = 200$ and $v_{in} = -0.1$.

We now compare the solutions of the full field equation (2.3) with those obtained from the collective coordinate model, Eqs. (3.27), using equivalent initial conditions. To do so, we examine the time evolution of the coordinates $x_i(t)$ and contrast them with the positions of the energy density peaks, $X_{\mathcal{E}_i}(t)$, associated with each sub-kink.

To determine $X_{\mathcal{E}_i}(t)$, we employ a time-slicing procedure. At each simulation time step t_s , the energy density $\mathcal{E}(t_s, z)$ is extracted from the numerical $K_4 - \bar{K}_4$ collision data. We then identify the χ_i localizations of the local maxima of $\mathcal{E}(t_s, z)$ at fixed t_s , which sets $X_{\mathcal{E}_i}(t_s) \equiv \chi_i$.

Figure (14) shows the coordinates evolution of an oscillon emerging from a $K_4 - \bar{K}_4$ collision. The collective coordinate approximation reproduces remarkably well the overall dynamical pattern observed in the full field results. In particular, the amplitud and long oscillation period of the sub-kinks closely match those obtained from the field equations of motion. The most noticeable discrepancy arises in the oscillation pattern of the central bion: while the field results exhibits a sharp frequency increase after the third bounce, this effect appears less pronounced in the collective coordinate model.

To investigate the long-time behavior of the oscillon, Fig. (15) shows the evolution of $x_i(t)$ and $X_{\mathcal{E}_i}(t)$ over an extended interval. Once again, the agreement between the two methods is very good. A characteristic feature is the abrupt reduction of the oscillon

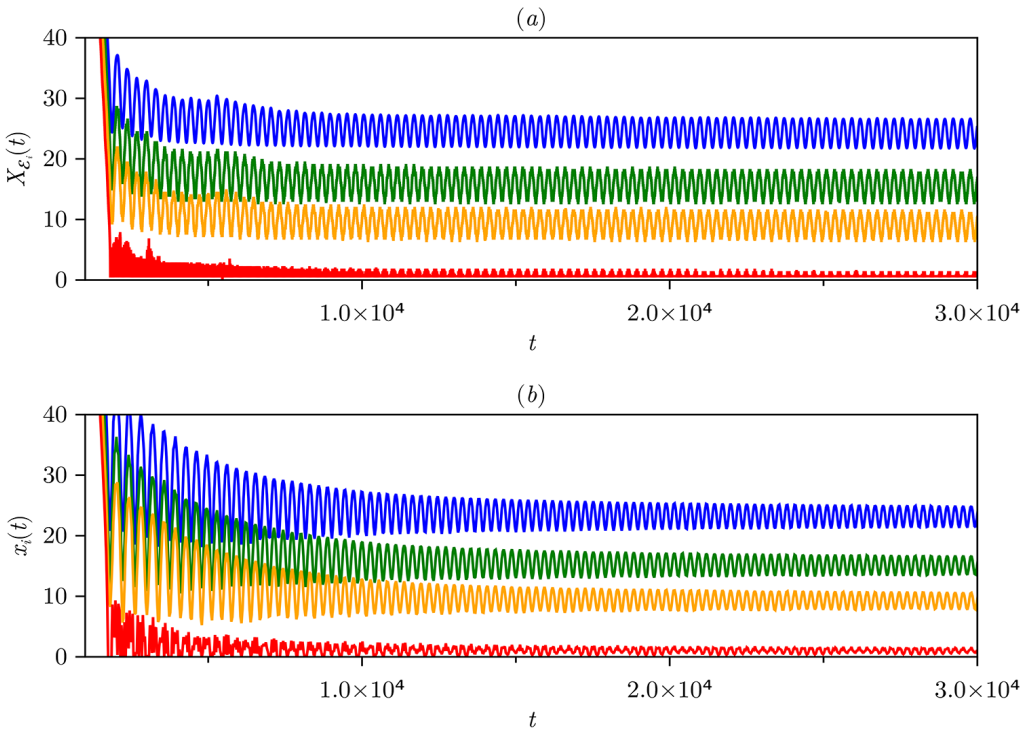


Figure 15. Oscillon evolution over a extended time period that includes the stable stage. Only positive values of the coordinates are displayed. The parameters values are $\alpha = 0.05$, $n = 4$, $L = 200$ and $v_{in} = -0.1$.

amplitude after a few initial bounces, from which the system settles into a long-lived, nearly stable configuration in which only a small amount of energy is radiated. During this stage, the oscillon maintains its shape and internal structure as it propagates, exhibiting an impressive degree of near-periodicity. This periodicity is evident in the Fourier spectra of the coordinates, displayed in Fig. (16), which show a set of narrow peaks, the dominant one, ω_1 , lying well below all relevant mass thresholds. Only small peaks associated with the outer sub-kinks penetrate above the mass threshold, indicating minimal radiative losses. The higher spectral frequencies correspond to overtones of the dominant mode, $\omega_j \approx j \omega_1$, $j = 1, 2, \dots$. This pattern is clearly visible in the $X_{\mathcal{E}_i}(\omega)$ spectra, and although less apparent in the $x_i(\omega)$ spectra, it is confirmed by inspecting the acceleration spectra $a_i(\omega)$, Fig. (8b), which also display the same overtones structure.

We highlight the emergence of a synchronization phenomenon, shown in Fig. (16), in which the sub-kinks adjust their internal oscillation modes and exhibit a coherent collective dynamics. This synchronization causes them to oscillate at shared frequencies, as evidenced by several of the resonant peaks in the spectra.

The results collected in table 1 reveal the impact of varying α on the oscillon properties. As discussed previously (see Fig. (16)), the slow modulation of the oscillon amplitude is governed by a large period T_L , which is extracted from the dominant low frequency ac-

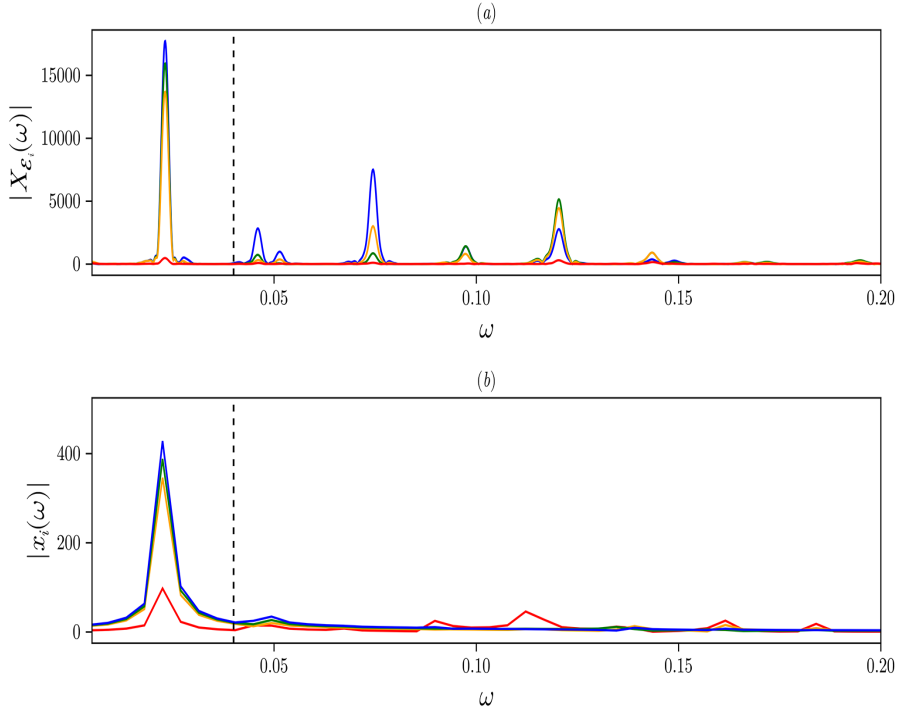


Figure 16. Fourier frequency spectra for the $X_{E_i}(\omega)$ and collective $x_i(\omega)$ coordinates, evaluated at later time at which the stable stage has been achieved $t = 100000$. The parameters selection is $\alpha = 0.05$, $n = 4$, $L = 200$ and $v_{in} = -0.1$.

cording to $T_L = 2\pi/\omega_1$, once the system reaches its stable oscillatory regime. In all cases we observe that T_L decreases as α increases, with a reasonable level of agreement between the collective coordinates predictions and the full field-theory results. A fit of $T_L(\alpha)$ to the field data yields the empirical expression

$$T_L \approx 80 \alpha^{-0.4}. \quad (4.2)$$

This scaling can be understood on physical grounds, if we introduce the ansatz $T_L = 2\pi/\omega_{\text{eff}}$, and assume that the effective oscillon frequency is controlled by the interaction of two relevant sub-kink pairs Eqs. (3.7,3.12), then $\omega_{\text{eff}} = (\omega_{-1,1} \omega_{k_{\frac{n}{2}}, \bar{k}_{-\frac{n}{2}}})^{1/2}$. This leads to the scaling $\omega_{\text{eff}} = g \alpha^{3/8}$, where $g = \left[\frac{\lambda m_1^3 C_{n,\alpha}}{\sqrt{2} \mu_{1,2} M_{\frac{k}{2}}} \right]^{1/4}$ is a slowly varying function of α , hence $T_L = 2\pi g^{-1} \alpha^{-3/8}$. The resulting power-law dependence is consistent with the empirical fit.

For the collective coordinate model, the oscillon lifetimes are estimated by assuming an exponential decay of the oscillon energy $E_{\text{CCM}}(t) = E_0 \exp\{-t/\tau\}$, during its stable stage, and fitting this expression to the numerical solutions of Eqs. (3.27,3.28). Within this framework, the eventual disappearance of the oscillon is consistent with a smooth, continuous decay of its energy toward the vacuum.

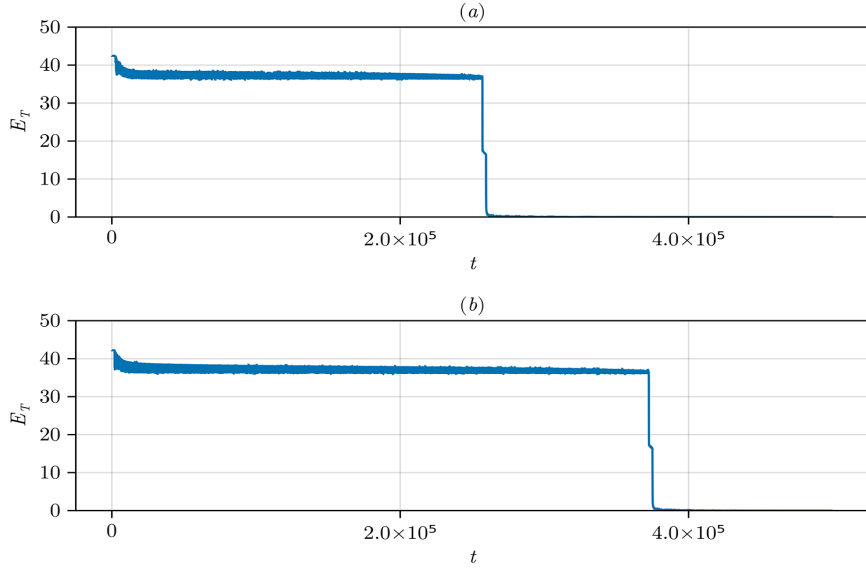


Figure 17. Total energy oscillon decay $E_T(t)$ for (a) $\alpha = 0.05$ and (b) $\alpha = 0.04$. The other parameters selection is $n = 4$, $L = 200$ and $v_{in} = 0.332$.

In contrast, the full field-theory simulations reveal a qualitatively different behavior. To visualize the oscillon's fate, we plot the total field energy $E(t)$ over very long time intervals, as shown in Figs. (17). The energy remains essentially constant throughout the oscillon's lifetime, until it suddenly collapses and the configuration rapidly decays into the vacuum. The results summarized in table 1 show that these oscillon's may persist for very long durations, *e.g.* for $\alpha = 0.01$, the life-time expands 5×10^5 oscillation cycles. We find that $\tau(\alpha)$ is also well fitted by a power-law given by $\tau \approx 5 \times \alpha^{-3.48}$. Combining this result with Eqs. (4.2), we obtain the following estimation for the oscillon's life-time cycles as

$$N_C = \frac{\tau}{T_L} \approx 0.06 \alpha^{-3.44}. \quad (4.3)$$

This power-law, is consistent with the results in table 1. But what is more interesting is that, extrapolating to smaller α values, suggests that the oscillons can be extremely long-lived, *e.g.* if $\alpha = 10^{-8}$, then $N_C = 10^{23}$ cycles. Although, nowadays results numerically impossible to simulate oscillon's evolution with so huge lifetimes, further analysis and comparison with other mechanisms that predict similar results [39] is worthwhile.

We also examine the effect of increasing the initial incident velocity on the $K_4 - \bar{K}_4$ collisions within both approaches. For $\alpha \leq 0.1$, we find that low incoming velocities typically lead to oscillon formation. However, when the impact velocity reaches $|v_i| \geq 0.25 - 0.3$ the collision generally becomes inelastic after the first bounce, the original multi-kinks separate and escape to infinity as illustrated in Fig. (7b,11b).

As noted earlier in the results of Fig. (11c, d), abrupt annihilations also occur at relatively short times for certain combinations of the parameters $\alpha - v_{in}$. These observations

Oscillon long-periods and life-times				
	FF	CCM	FF	CCM
α	T_L	T_L	τ	τ
0.01	862	665	4.6×10^7	1.8×10^5
0.02	556	460	4.1×10^6	9.7×10^4
0.03	346	360	9.9×10^5	8.2×10^4
0.04	302	322	3.8×10^5	5.4×10^4
0.05	272	275	2.8×10^5	4.5×10^4
0.06	258	244	6.1×10^4	3.9×10^4
0.07	243	232	3.5×10^4	3.5×10^4
0.08	230	218	2.6×10^4	3.1×10^4
0.09	225	202	2.0×10^4	2.8×10^4
0.1	204	196	2.7×10^4	2.5×10^4

Table 1. Oscillon large periods T_L and life-times τ as a function of α , obtained from the full field (FF) or collective coordinate (CCM) schemes.

are indicative of a likely non uniform or chaotic mechanism that triggers the sudden disappearance of the $K_4 - \bar{K}_4$ configuration, a subject that clearly deserves further study.

5 Conclusions

The aim of this work was to construct a commensurable and non-degenerate double sine-Gordon theory that exhibits a rich phenomenology, enabling the exploration of novel multi-soliton and oscillon properties. In the degenerate limit $\alpha = 0$, the model supports n kink solutions interpolating between consecutive absolute minima. In contrast, moving into the $\alpha > 0$ regime induces a partial lifting of the vacuum degeneracy, providing a natural mechanism for the emergence of static multi-kinks K_n composed of an arbitrary number n of internal sub-kinks. Although exact analytical field configurations could not be obtained, the smooth-modulation approximation performs remarkably well and allows for a detailed and comprehensive analysis of the multi-kink sector.

The multi-kink K_n is characterized by a topological charge $Q_n = n$, equal to the sum of the individual sub-kink charges, and by a mass $M_{K(n,\alpha)}$ [Eqs. (2.18,2.21)], which results from adding the sub-kink masses [Eq. (2.19)] together with a binding-energy contribution $\Delta_{K(n,\alpha)}$ [Eq. (2.20)]. In the large- n limit, all these quantities scale linearly with n . The multi-kink structure, with its well-defined internal energy lumps, becomes particularly clear in the small- α regime, where we identified the following scaling relations: (a) the equilibrium distance between adjacent sub-kinks obeys $\xi_{i+1} - \xi_i \approx \frac{1}{m_i} \log(\frac{\text{const}}{\alpha})$ Eqs. (3.5,2.25); (b) the total size satisfies $\sigma_{K(n,\alpha)} \approx \frac{2n}{\pi} \ln(n) \ln(\frac{32}{\alpha})$ Eq. (2.30); and (c) the binding energy scales as $\Delta V_{K(n,\alpha)} \approx \frac{2n}{\pi} \alpha \ln(\frac{12}{\alpha})$ Eq. (2.22). Thereby, we can visualize the multi-kink as a large size, weakly bound n -soliton.

For the $K_4 - \bar{K}_4$ scattering, we identified three distinct dynamical regimes: (a) Rapid annihilation, occurring after only a few bounces; (b) Inelastic dispersion, in which the colliding configurations bounce back and separate to infinity. Unlike the familiar behavior of the ϕ^4 , ϕ^6 , and related models [5, 8, 20–22, 49], no multi-bounce escape windows were observed.

However, our exploration has so far covered only a restricted region of the full $\{n, \alpha, v_i\}$ parameter space, so such structures cannot be excluded; (c) The formation of long-lived compound oscillons, which constitutes the most novel outcome. These composite oscillons reflect the internal structure of the parent multi-kinks and therefore possess multiple characteristic scalar masses [Eq. (2.10)] and resonant oscillation frequencies [Eqs. (3.7,3.12)]. These features distinguishes them from most oscillons reported in the literature.

We also developed a collective coordinate model that offers a good approximation to the full field dynamics during multi-kink collisions. Its construction involves several key elements: the use of dynamical Bogomol'nyi relations to determine the inter-sub-kink forces [Eq. (3.2)] and the $K_4 - \bar{K}_4$ interaction force [Eq. (3.11)]; and the formulation of an approximate radiation scheme that exploits the fact that the oscillation frequencies of the internal sub-kinks lie below the radiation threshold. As a result, radiation losses arise predominantly from the external sub-kinks, giving rise to an effective radiation-reaction force [Eq. (3.23)]. All these components are incorporated into the equations defining the collective coordinate model [Eq. (3.27)].

The field-theoretic solutions, together with those obtained from the collective coordinate model, provide a compelling characterization of the oscillons observed in this work. They emerge as large-amplitude, long-lived configurations in which the sub-kinks synchronize with remarkable quasi-periodicity. Particularly noteworthy is Eq. (4.3), which suggest that for $\alpha \ll 1$ the oscillon lifetime could become extraordinarily large.

As discussed, incorporating radiation effects into the collective coordinate framework is crucial for reproducing many of the oscillon properties obtained from the full field dynamics. However, the eventual fate of the oscillon, especially its abrupt collapse, cannot be accounted for by a linearized radiation mechanism alone. Understanding this phenomenon will likely require additional ingredients, such as non-linear effects that become relevant near the instability threshold, and therefore represents an important direction for future study.

Overall, the results presented here outline a rich scenario that merits further exploration. They may provide insights into the emergence of coherent structures in physical systems [15, 50], and they also suggest that extending the non-degenerate double sine-Gordon model, or similar constructions, to higher spatial dimensions, possibly including gauge fields, is a promising topic for future research.

References

- [1] N. Manton and P. Sutcliffe, *Topological Solitons.*, Cambridge Monographs on Mathematical Physics, United Kingdom (2004).
- [2] T. Vachaspati, *Kinks and Domain Walls: An Introduction to Classical and Quantum Solitons*, Cambridge University Press (2006), [10.1017/CBO9780511535192](https://doi.org/10.1017/CBO9780511535192).
- [3] E. Weinberg, *Classical Solutions in Quantum Field Theory: Solitons and Instantons in High Energy Physics.*, Cambridge Monographs on Mathematical Physics, United Kingdom (2012).
- [4] R.F. Dashen, B. Hasslacher and A. Neveu, *Nonperturbative methods and extended-hadron models in field theory. ii. two-dimensional models and extended hadrons*, *Phys. Rev. D* **10** (1974) 4130.

- [5] D.K. Campbell, J.F. Schonfeld and C.A. Wingate, *Resonance structure in kink-antikink interactions in ϕ^4 theory*, *Physica D: Nonlinear Phenomena* **9** (1983) 1.
- [6] P.G. Kevrekidis and J. Cuevas-Maraver, *Historical A Dynamical Perspective on the ϕ^4 Model: Past, Present and Future*, Springer Cham, Switzerland (2019).
- [7] V. Makhankov, *Dynamics of classical solitons in non-integrable systems*, *Physics Reports* **35** (1978) 1.
- [8] M. Moshir, *Soliton-antisoliton scattering and capture in the ϕ^4 theory*, *Nuclear Physics B* **185** (1981) 318.
- [9] P. Anninos, S. Oliveira and R.A. Matzner, *Fractal structure in the scalar $\lambda(\phi^2 - 1)^2$ theory*, *Phys. Rev. D* **44** (1991) 1147.
- [10] F. Simas, A. Gomez, K. Nobrega and J. Oliveira, *Suppression of two-bounce windows in kink-antikink collisions.*, *Journal of High Energy Physics* **2016** (2016) 1.
- [11] T. Sugiyama, *Kink-antikink collisions in the two-dimensional ϕ^4 model*, *Prog Theor Phys* **61** (1979) 1550.
- [12] I. Takyi and H. Weigel, *Collective coordinates in one-dimensional soliton models revisited*, *Phys. Rev. D* **94** (2016) 085008.
- [13] N.S. Manton, K. Oleś, T. Romańczukiewicz and A. Wereszczynski, *Kink moduli spaces: Collective coordinates reconsidered*, *Phys. Rev. D* **103** (2021) 025024.
- [14] N.S. Manton, K. Oleś, T. Romańczukiewicz and A. Wereszczynski, *Collective coordinate model of kink-antikink collisions in ϕ^4 theory*, *Phys. Rev. Lett.* **127** (2021) 071601.
- [15] A. Scott, *Nonlinear Science: Emergence and Dynamics of Coherent Structures*, Oxford University Press, United Kingdom (2003).
- [16] J. Cuevas-Maraver, P.G. Kevrekidis and F. Williams, *The sine-Gordon Model and its Applications: From Pendula and Josephson Junctions to Gravity and High-Energy Physics*, Springer Cham, Switzerland (2014).
- [17] M.J. Ablowitz, D.J. Kaup, A.C. Newell and H. Segur, *Method for solving the sine-gordon equation*, *Phys. Rev. Lett.* **30** (1973) 1262.
- [18] V. Zakharov, L. Takhtajan and L. Faddev, *Complete description of solutions of the the sine-gordon equation*, *Doklady AN SSSR* **219** (1973) 1334.
- [19] D.K. Campbell, M. Peyrard and P. Sodano, *Kink-antikink interactions in the double sine-gordon equation*, *Physica D: Nonlinear Phenomena* **19** (1986) 165.
- [20] P. Dorey, K. Mersh, T. Romanczukiewicz and Y. Shnir, *Kink-antikink collisions in the ϕ^6 model*, *Phys. Rev. Lett.* **107** (2011) 091602.
- [21] A. Demirkaya, R. Decker, P.G. Kevrekidis, I.C. Christov and A. Saxena, *Kink dynamics in a parametric ϕ^6 system: a model with controllably many internal modes*, *Journal of High Energy Physics* **2017** (2017) 1.
- [22] A. Moradi Marjaneh, V.A. Gani, D. Saadatmand, S.V. Dmitriev and K. Javidan, *Multi-kink collisions in the ϕ^6 model*, *Journal of High Energy Physics* **2017** (2017) 28.
- [23] V.A. Gani, A.M. Marjaneh and P.A. Blinov, *Explicit kinks in higher-order field theories*, *Phys. Rev. D* **101** (2020) 125017.

[24] A. Khare, I.C. Christov and A. Saxena, *Successive phase transitions and kink solutions in ϕ^8 , ϕ^{10} and ϕ^{12} field theories*, *Phys. Rev. E* **90** (2014) 023208.

[25] F. Suzuki and W.H. Zurek, *Topological defect formation in a phase transition with tunable order*, *Phys. Rev. Lett.* **132** (2024) 241601.

[26] N.S. Manton, *Forces between kinks and antikinks with long-range tails*, *Journal of Physics A: Mathematical and Theoretical* **52** (2019) 065401.

[27] I.C. Christov, R.J. Decker, A. Demirkaya, V.A. Gani, P.G. Kevrekidis, A. Khare et al., *Kink-kink and kink-antikink interactions with long-range tails*, *Phys. Rev. Lett.* **122** (2019) 171601.

[28] E. Belendryasova and V.A. Gani, *Scattering of the ϕ^8 kinks with power-law asymptotics*, *Communications in Nonlinear Science and Numerical Simulation* **67** (2019) 414.

[29] I.C. Christov, R.J. Decker, A. Demirkaya, V.A. Gani, P. Kevrekidis and A. Saxena, *Kink-antikink collisions and multi-bounce resonance windows in higher-order field theories*, *Communications in Nonlinear Science and Numerical Simulation* **97** (2021) 105748.

[30] N.H. Christ and T.D. Lee, *Quantum expansion of soliton solutions*, *Phys. Rev. D* **12** (1975) 1606.

[31] d.S.A. de Brito G.P., *Multikink solutions and deformed defects*, *Annals of Physics* **351** (2014) 620.

[32] J. Lozano-Mayo and M. Torres-Labansat, *Kink solutions in a generalized scalar ϕ_g^4 field model*, *Journal of Physics Communications* **5** (2021) 025004.

[33] P. Dorey, A. Gorina, T. Romańczukiewicz and Y. Shnir, *Collisions of weakly-bound kinks in the christ-lee model*, *Journal of High Energy Physics* **2023** (2023) 1.

[34] C. Halcrow, R.R. John and A. N., *Modified sine-gordon theory with static multikinks*, *Phys. Rev. D* **110** (2024) 065010.

[35] M. Gleiser, *Pseudostable bubbles*, *Phys. Rev. D* **49** (1994) 2978.

[36] E.W. Kolb and I.I. Tkachev, *Large-amplitude isothermal fluctuations and high-density dark-matter clumps*, *Phys. Rev. D* **50** (1994) 769.

[37] N. Graham, *An electroweak oscillon*, *Phys. Rev. Lett.* **98** (2007) 101801.

[38] M.A. Amin and D. Shirokoff, *Flat-top oscillons in an expanding universe*, *Phys. Rev. D* **81** (2010) 085045.

[39] J. Ollé, O. Pujolàs and F. Rompineve, *Recipes for oscillon longevity*, *Journal of Cosmology and Astroparticle Physics* **2021** (2021) 015.

[40] E. Bogomolny, *The stability of classical solutions*, *Sov. J. Nucl. Phys.* **24** (1976) 449.

[41] L.J. Boya and J. Casahorran, *General scalar bidimensional models including kinks*, *Annals of Physics* **196** (1989) 361 .

[42] N.S. Manton, *Integration theory for kinks and sphalerons in one dimension*, *J. Phys. A* **57** (2023) 025202.

[43] A. Alonso-Izquierdo, S. Navarro-Obregón, K. Oles, J. Queiruga, T. Romanczukiewicz and A. Wereszczynski, *Semi-bogomol'nyi-prasad-sommerfield sphaleron and its dynamics*, *Phys. Rev. E* **108** (2023) 064208.

- [44] R.H. Goodman and R. Haberman, *Chaotic scattering and the n -bounce resonance in solitary-wave interactions*, *Phys. Rev. Lett.* **98** (2007) 104103.
- [45] N.S. Manton and H. Merabet, *kinks - gradient flow and dynamics*, *Nonlinearity* **10** (1997) 3.
- [46] P. Dorey, T. Romańczukiewicz and Y. Shnir, *Staccato radiation from the decay of large amplitude oscillons*, *Physics Letters B* **806** (2020) 135497.
- [47] S. Navarro-Obregón, L.M. Nieto and J.M. Queiruga, *Inclusion of radiation in the collective coordinate method approach of the ϕ^4 model*, *Phys. Rev. E* **108** (2023) 044216.
- [48] N.F. Smyth and A.L. Worthy, *Soliton evolution and radiation loss for the sine-gordon equation*, *Phys. Rev. E* **60** (1999) 2330.
- [49] P. Dorey, A. Gorina, I. Perapechka, T. Romańczukiewicz and Y. Shnir, *Resonance structures in kink-antikink collisions in a deformed sine-gordon model*, *Journal of High Energy Physics* **2021** (2021) 1.
- [50] N. Xu, J. Chen, Y.-P. Zhang and Y.-X. Liu, *Multikink brane in gauss-bonnet gravity and its stability*, *Phys. Rev. D* **107** (2023) 124011.